Lithos 112S (2009) 385–399

Contents lists available at ScienceDirect

Lithos

journal homepage: www.elsevier.com/locate/lithos

The newly discovered Jurassic Tikiusaaq carbonatite-aillikite occurrence, West Greenland, and some remarks on carbonatite–kimberlite relationships

Sebastian Tappe [a,b,*], Agnete Steenfelt [c], Larry M. Heaman [a], Antonio Simonetti [d]

[a] Department of Earth and Atmospheric Sciences, University of Alberta, 1-26 Earth Sciences Building, Edmonton, Alberta, Canada T6G 2E3
[b] De Beers Canada Inc., 300-65 Overlea Boulevard, Toronto, Ontario, Canada M4H 1P1
[c] Geological Survey of Denmark and Greenland, Øster Voldgade 10, DK-1350, Copenhagen, Denmark
[d] Department of Civil Engineering and Geological Sciences, University of Notre Dame, 156 Fitzpatrick Hall, Notre Dame, Indiana 46556, USA

ARTICLE INFO

Article history:
Received 1 October 2008
Accepted 2 March 2009
Available online 20 March 2009

Keywords:
U–Pb geochronology
Mineral chemistry
Intrusive carbonatite
Ultramafic lamprophyre
Continental rifting
North Atlantic craton

ABSTRACT

We discuss mineral chemistry data and report ten high-precision U–Pb (zircon, baddeleyite, pyrochlore, and perovskite) and Rb–Sr phlogopite ages for the newly discovered Tikiusaaq carbonatite intrusion and associated ultramafic dykes from the North Atlantic craton, West Greenland. At Tikiusaaq, massive dolomite-calcite carbonatite sheets intruded an 2×3 km area along a ductile shear zone between ca. 158 and 155 Ma. The accompanying carbonatite and carbonate-rich ultramafic silicate dykes were emplaced between ca. 165 and 157 Ma in close proximity to this carbonatite centre utilizing pre-existing brittle fractures. The deep volatile-rich magmatism at Tikiusaaq forms part of a larger Jurassic alkaline province in southern West Greenland and represents the earliest manifestation of rifting processes related to the opening of the Mesozoic–Cenozoic Labrador Sea Basin.

Although the ultramafic silicate dykes macroscopically resemble hypabyssal kimberlites, they are identified as kimzeyite-bearing monticellite aillikites (carbonate-rich ultramafic lamprophyres) using a modern mineralogical–genetic classification. The overlapping emplacement ages of the carbonatite sheets and aillikite dykes, along with the carbonate-rich nature of the latter, suggest a genetic relationship between these magma types. The aillikites carry garnet peridotite xenoliths and have mineralogical characteristics of primitive magmas such as highly forsteritic olivine (up to Fo_{90} mol%) and Cr-rich spinel (up to 46 wt.% Cr_2O_3) microphenocrysts; whereas the carbonatite sheets reveal a higher degree of differentiation such as Fe-rich dolomite compositions (up to 9 wt.% FeO). The initial findings reported here from Tikiusaaq suggest that a link between these magma types by an increasing degree of partial melting of a common carbonated upper mantle peridotite source region, as commonly envisaged for the compositionally similar Sarfartoq complex, is untenable. Rather, proto-aillikite magma may be parental to the dolomitic carbonatite sheets, but the nature of the carbonate separation mechanism(s) is presently not understood.

1. Introduction

Ever since Brøgger (1921) first proposed the magmatic origin of carbonatites, scientific interest in this magma type has outweighed its volumetric significance. Many studies have highlighted the important role of the various associated alkaline silicate rock types in carbonatite magma petrogenesis and this diversity appears to reflect that carbonatite magma is produced in a number of ways (Bell, 1998; Mitchell, 2005; Woolley and Kjarsgaard, 2008). Aillikites — *or carbonate-rich ultramafic lamprophyres* — are among the rarest and compositionally most extreme magma types associated with carbonatites (Rock, 1986; Mitchell et al., 1999; Tappe et al., 2005). They are characterized by abundant primary groundmass carbonate and strong SiO_2 undersaturation; in some cases aillikites modally grade into carbonatites (Malpas et al., 1986; Mitchell et al., 1999; Tappe et al., 2006). The absence of a wide compositional gap between carbonatites and aillikites contrasts with virtually all other known carbonatite–alkaline silicate rock associations; this rather gradational nature has been ascribed to an increasing degree of partial melting of carbonated peridotite, i.e., a primary melting relationship (Dalton and Presnall, 1998; Mitchell et al., 1999; Mitchell, 2005; Woolley and Kjarsgaard, 2008; Foley et al., this issue). However, there is no a priori reason why these continuous gradations could not result from magmatic differentiation as discussed in Larsen and Rex (1992) and Tappe et al. (2006).

Southern West Greenland is one of the key regions where the carbonatite–aillikite association occurs (Larsen and Rex, 1992; Mitchell et al., 1999; Upton et al., 2003; Tappe et al., 2005) and glacially abraded bedrock exposures offer splendid opportunities for studying its nature.

* Corresponding author. Department of Earth and Atmospheric Sciences, University of Alberta, 1-26 Earth Sciences Building, Edmonton, Alberta, Canada T6G 2E3. Tel.: +1 780 4924354; fax: +1 780 4922030.
E-mail addresses: sebastian.tappe@ualberta.ca, sebastian.tappe@ca.debeersgroup.com (S. Tappe).

0024-4937/$ – see front matter © 2009 Elsevier B.V. All rights reserved.
doi:10.1016/j.lithos.2009.03.002

However, some important petrogenetic aspects of this relationship are still not fully understood due to; (1) the lack of high-precision emplacement ages for both carbonatite and aillikite phases from an individual occurrence, and (2) the uncertainty about whether the carbonatites represent near-primary liquids or liquids produced by secondary processes such as fractional crystallization and immiscibility, or are not liquid compositions at all. An additional complicating factor to unravelling petrogenetic links between carbonatites and aillikites — or ultramafic lamprophyres (UML) in the broadest sense — is that the latter are too often confused or lumped together with kimberlites (Emeleus and Andrews, 1975; Alibert and Albarede, 1988; Bizzarro et al., 2002; Gaffney et al., 2007; Hutchison and Heaman, 2008), which simply ignores their distinct volatile composition and alkali contents (Kjarsgaard et al., this issue). This has led unnecessarily to over-emphasis of carbonatite–kimberlite relationships and provoked extreme ideas such as kimberlites are merely peridotite-contaminated carbonatites (Nielsen and Sand, 2008; Patterson et al., this issue). The dilemma becomes most obvious in paraphrasing Dalton and Presnall (1998) that the Sarfartoq complex of West Greenland, which is a classic carbonatite-aillikite occurrence, is the best natural analogue of their experimentally produced carbonatitic–kimberlitic melt continuum.

In this paper we report results on the age, geology, and mineralogy of the newly discovered West Greenland 'Tikiusaaq' carbonatite complex and its accompanying ultramafic dyke rocks (Steenfelt et al., 2006; Steenfelt et al., 2007). Based on the mineral assemblage (e.g., presence of kimzeyite) and mineral compositional trends (e.g., spinel and phlogopite) the ultramafic dyke rocks are more akin to type aillikites from Aillik Bay in Labrador, North Atlantic craton (NAC) than to archetypal Kaapvaal and Slave craton kimberlites. Our high-precision U–Pb and Rb–Sr age data demonstrate that carbonatite and aillikite magmatism at Tikiusaaq was contemporaneous with and occurred as a distal effect of rift initiation in the developing Labrador Sea Basin during the Middle Jurassic. The prime goal of this paper is to lay the groundwork for further detailed petrological studies on the Tikiusaaq intrusion that will certainly enable us to more rigorously test prevailing ideas about petrogenetic links between carbonatites, aillikites, and the alleged kimberlites in areas of rifted cratonic lithosphere.

2. Carbonatite-aillikite magmatism of southern West Greenland

The Archean and Paleoproterozoic crust of southern West Greenland (Fig. 1a) has been repeatedly subjected to mantle-derived

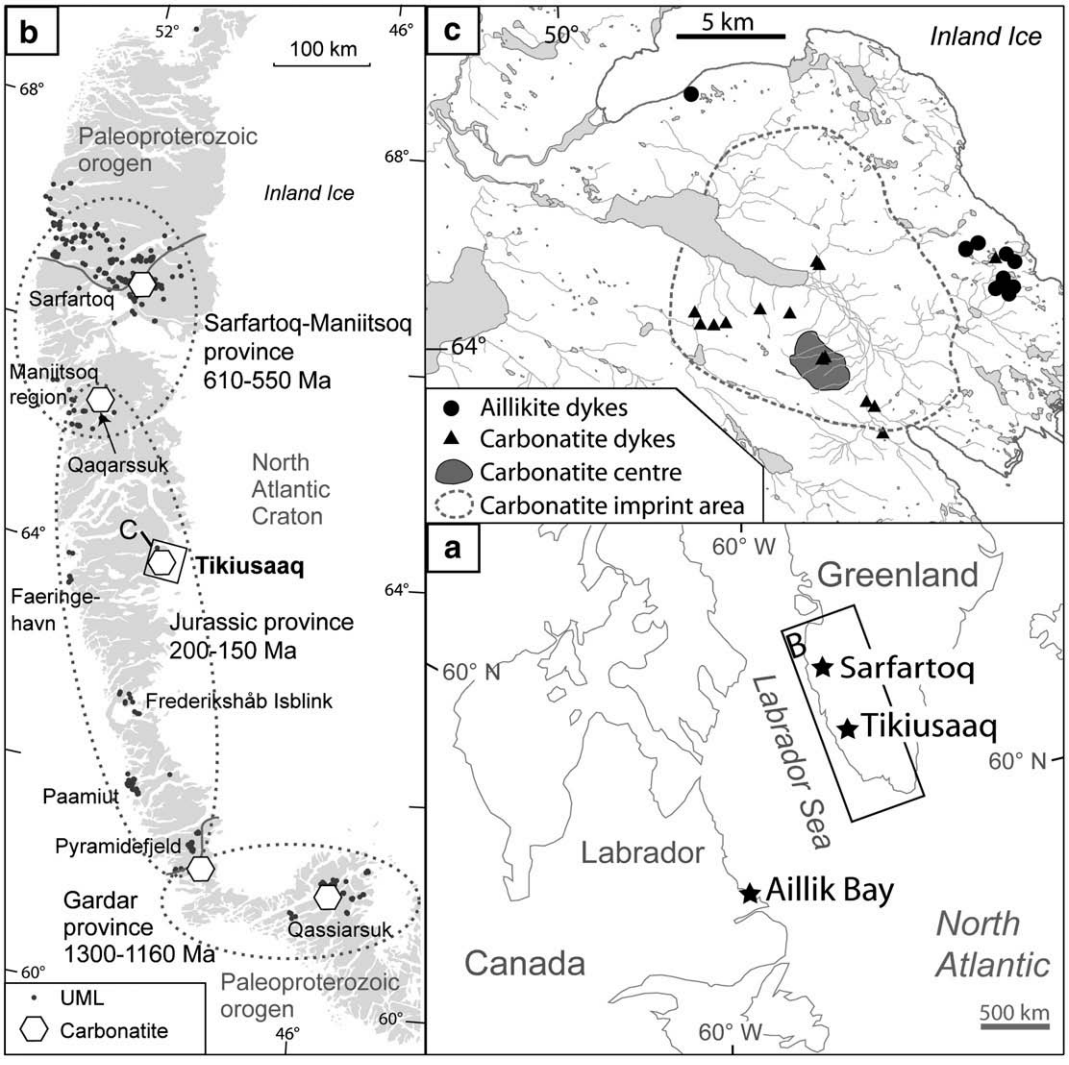

Fig. 1. Location of the newly discovered Tikiusaaq carbonatite-aillikite occurrence in southern West Greenland. (a) Tikiusaaq location in the greater North Atlantic cratonic region including the aillikite type locality at Aillik Bay in Labrador. (b) Distribution of carbonatite-aillikite occurrences across southern West Greenland. Symbols for carbonatites are not to scale. Note that the Jurassic carbonatite-aillikite province (200–150 Ma) occurs in the central part of the North Atlantic craton; whereas the Neoproterozoic (610–550 Ma) and Mesoproterozoic (1300–1160 Ma) carbonatite provinces are confined to the craton margins in the north and south, respectively. (c) Outline of the Jurassic Tikiusaaq carbonatite intrusion and associated aillikite dykes at 64°N close to the inland ice margin. A sample list is provided in Electronic Annex 2.

Table 1
Estimated range of modal mineral abundances (vol.%) of Tikiusaaq carbonatites and aillikites, West Greenland.

Mineral Rock type	Ol	Mtc	Cpx	Phl	Amph	Opaques	Prv	Ap	Pcl	Cal/Dol
Carbonatite sheets										
Calciocarbonatite	x	–	–	x-4	x	x-6	–	x-10	0–1	60–95/5–30
Magnesiocarbonatite	–	–	–	x-4	x	x-6	–	x-10	0–1	5–35/50–90
Carbonatite dykes[a]	0–5	–	x-5	5–15	2–15	2–10	–	1–3	–	5–20/5–50
Aillikite dykes	10–30	0–20	0–5	2–15	–	10–15	x-3	x-2	–	5–20/x

x = Minor amounts; – = not detected; symbols for minerals according to Kretz (1983) except for Pcl — pyrochlore.
The carbonatite sheets and dykes may contain trace amounts of zircon, baddeleyite, rutile, and Fe-sulphides.
The aillikite dykes may contain Ti-rich primary garnets of kimzeyitic composition.
[a] The carbonatite dykes may contain up to 10% country rock fragments.

carbonatite magmatism (Larsen and Rex, 1992) that, at least in some areas, originated from depths greater than 150 km, well within the diamond stability field (e.g., Nielsen and Sand, 2008). This magmatic activity includes three major carbonatite-aillikite intrusive periods (Fig. 1b), all of which are associated with rifting of the NAC lithosphere (Tappe et al., 2007, and references therein): (1) ca. 1300–1160 Ma; e.g., Qassiarsuk; (2) ca. 610–550 Ma; e.g., Sarfartoq; and (3) ca. 200–150 Ma; e.g., Qaqarssuk. The Tikiusaaq intrusion forms part of the 'youngest' Jurassic carbonatite-aillikite magmatic activity; it was discovered in 2005 in a poorly exposed area close to the inland ice margin at 64°N approximately 150 km to the southeast of Nuuk (Steenfelt et al., 2006, 2007). The magmas were emplaced into Neoarchean gneisses and supracrustal sequences at the northern boundary of the Tasiusarsuaq terrane in the central part of the NAC and for a summary of the regional Archean geology the reader is referred to Friend et al. (1996).

3. Results

3.1. Intrusive units, rock types, and terminology

Three main intrusive units listed in order of decreasing carbonate content form part of the newly discovered Tikiusaaq carbonatite intrusion: (1) massive carbonatite sheets, (2) carbonatite dykes typically containing country rock fragments, and (3) aillikite dykes. No cross-cutting field relationships between these intrusive units were

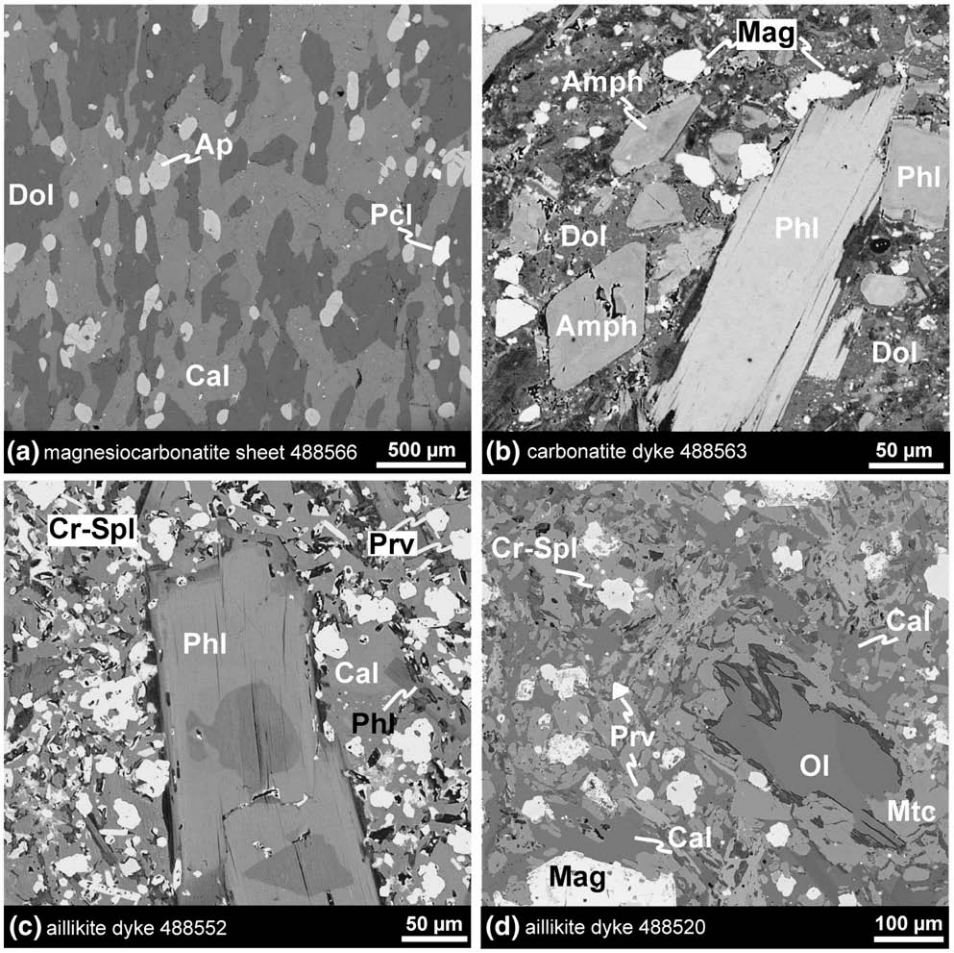

Fig. 2. Backscattered electron images of the Tikiusaaq carbonatites and aillikites. (a) mixed dolomite-calcite carbonatite sheet (magnesiocarbonatite). Note the elongate interlocking carbonate grains and concentration of apatite and pyrochlore crystals in discrete bands. (b) Carbonatite dyke exhibiting phlogopite and calcic amphibole microphenocrysts set in a dolomite matrix. (c) Aillikite dyke exhibiting zoned phlogopite microphenocryst set in a calcite and spinel dominated matrix. (d) Aillikite dyke showing zoned olivine microphenocryst partly replaced by groundmass monticellite. Note the abundant groundmass calcite and perovskite, but the absence of serpentine. Mineral abbreviations follow Kretz (1983) except for pyrochlore (Pcl).

observed. Ranges of estimated modal mineral abundances of rock types comprising these intrusive units are listed in Table 1.

3.1.1. Carbonatite sheets

Massive carbonatite sheets appear to be confined to a 2×3 km area that is hereafter referred to as the 'carbonatite centre' (Fig. 1c). The emplacement of the carbonatite sheets occurred into a ductile shear zone and caused variable degrees of fracturing, carbonate coating, and alteration of the Archean country rocks over a >10×10 km area. This large dimension of carbonatite imprint may suggest that the presently exposed carbonatite sheets represent only the roof parts of an even larger intrusion and/or the presence of currently unexposed satellite intrusions. More likely, however, is that protracted fluid-flow that was related to the carbonatite magmatism occurred into the shear zone and produced this comparatively large halo. The 2-to-50 m thick carbonatite sheets are interleaved with slivers of Archean gneiss and amphibolite, which are in part metasomatically altered, i.e., reaction-lined with glimmerite stringers. Internal veining of the carbonatite sheets and the presence of a late-stage carbonatite breccia phase indicates that multiple magma pulses were involved. The carbonatite breccia consists of coarse, irregular carbonatite and glimmerite (phlogopite, apatite, and magnetite) fragments in a fine-grained, carbonate-dominated matrix suggestive of scavenging of early carbonatite sheets.

The carbonatite sheets have variable grain size ranging from <1 mm to cm-size. Elongate, interlocking carbonate grains typically cause some degree of vertical orientation (Fig. 2a) that is pronounced by concentration of non-carbonate minerals in discrete bands and variation of carbonate mineral grain size. A few samples contain anhedral, cm-sized calcite blasts/megacrysts set in a finer matrix that consists of elongate interlocking carbonate grains. Rare cm-wide, fine-grained carbonate veinlets, mineralogically clearly distinct from the carbonatite dykes described in Section 3.1.2., were observed cutting the carbonatite sheets. The absence of non-carbonate minerals such as phlogopite and their mosaic textures suggest precipitation from late-stage CO_2-liquids and/or fluids.

Based on mineralogy and following the recommendations in Le Maitre (2002), two carbonatite varieties comprise the sheet intrusion(s): (1) calcite carbonatite and (2) dolomite carbonatite. However, it is imperative to note that the vast majority of carbonatites examined during this study consist of variable mixtures of calcite and dolomite and that only a few examples with either calcite or dolomite

Table 2
ID–TIMS U–Pb baddeleyite, pyrochlore, and perovskite, as well as Rb–Sr results for Tikiusaaq carbonatite sheets and aillikite dykes, North Atlantic craton, West Greenland.

Description*	Weight (μg)	U (ppm)	Th (ppm)	Pb (ppm)	Th/U	TCPb (pg)	**$^{206}Pb/^{238}U$	**$^{207}Pb/^{235}U$	**$^{207}Pb/^{206}Pb$	Apparent ages (Ma) $^{206}Pb/^{238}U$	Apparent ages (Ma) $^{207}Pb/^{235}U$
Calciocarbonatite sheet 488516											
1. Bdl, reddish brown subhedral flakes, 50–100 μm (7)	6.0	253	13.6	9.79	0.054	24.3	0.02467±20	0.19449±1267	0.05718±350	157.1±1.3	180.5±10.7
2. Bdl, reddish brown subhedral flakes, 50–100 μm (3)	5.3	121	n.a.	5.85	n.a.	17.0	0.02466±47	0.07783±1680	0.02289±482	157.0±2.9	76.1±15.7
Magnesiocarbonatite sheet 488523											
1. Pcl, yellow-to-orange octahedrons, 150–200 μm (2)	12.7	58655	1211	1355	0.021	488	0.02471±4	0.16904±30	0.04962±6	157.3±0.3	158.6±0.3
2. Pcl, yellow-to-orange octahedrons, 150–200 μm (4)	51.5	6764	3877	219	0.573	2014	0.02493±6	0.16895±111	0.04914±32	158.8±0.4	158.5±1.0
3. Pcl, reddish octahedrons, 150–200 μm (3)	29.5	20693	934	526	0.045	1198	0.02563±4	0.17481±40	0.04946±11	163.1±0.3	163.6±0.4
Aillikite dyke 488520											
1. Prv, brown octahedrons, 80–200 μm (80)	189	214	1998	23.9	9.34	542	0.02511±47	0.16764±422	0.04842±84	159.9±3.0	157.4±3.7
Aillikite dyke 488546											
1. Prv, brown octahedrons, 60–120 μm (80)	188	74.7	88.3	7.20	1.18	366	0.02539±16	0.16704±467	0.04772±136	161.6±1.0	156.8±4.1
2. Prv, brown octahedrons, 50–100 μm (120)	274	70.2	181	6.60	2.58	512	0.02574±16	0.16996±474	0.04789±136	163.8±1.0	159.4±4.1
Aillikite dyke 488548											
1. Prv, brown octahedrons, 80–120 μm (130)	273	44.6	n.a.	5.80	n.a.	713	0.02607±35	0.16229±1084	0.04514±307	165.9±2.2	152.7±9.4

Sample description	Rb (ppm)	Sr (ppm)	$^{87}Rb/^{86}Sr$	***$2\sigma_m$	$^{87}Sr/^{86}Sr$	***$2\sigma_m$
Calciocarbonatite sheet 459126						
[a]157.4±1.3 Ma (2σ), MSWD=0.15, $^{87}Sr/^{86}Sr_i$=0.70373±3						
A. Phlogopite phenocryst, greenish brown, <3×2×1 mm	253.9	26.38	28.02	±0.42	0.765470	±0.000038
B. Phlogopite phenocryst, greenish brown, <3×2×1 mm	240.1	25.34	27.58	±0.41	0.764590	±0.000038
C. Phlogopite phenocryst, greenish brown, <3×2×1 mm	291.8	30.28	28.05	±0.42	0.765880	±0.000038
Bulk-rock	10	3563	0.008	±0.0001	0.703747	±0.000035
Aillikite dyke 493334						
[a]157.9±1.1 Ma (2σ), MSWD=0.65, $^{87}Sr/^{86}Sr_i$=0.70369±4						
A. Phlogopite macrocryst, dark brown, 6×5×2 mm	269.5	65.14	12.00	±0.18	0.730340	±0.000037
B. Phlogopite macrocryst, dark brown, 6×5×1 mm	312.9	66.89	13.57	±0.20	0.733580	±0.0001
C. Phlogopite macrocryst, light brown, 3×3×1 mm	362.6	71.81	14.65	±0.22	0.736060	±0.00007
D. Phlogopite macrocryst, light brown, <3×3×1 mm	298.8	60.47	14.34	±0.22	0.735390	±0.000037
E. Phlogopite macrocryst, light brown, <3×3×1 mm	335	65.44	14.86	±0.23	0.736940	±0.00006
Bulk-rock	41.32	1871	0.062	±0.001	0.703828	±0.000035

*Bdl — baddeleyite, pcl — pyrochlore, prv — perovskite; no. in parentheses are numbers of grains analysed.
**Atomic ratios corrected for fractionation, blank (1 pg Pb; 0.5 pg U), isotopic tracer, and common Pb.
TCPb is estimated total initial common Pb based on the Stacey & Kramers (1975) Pb evolution model; uncertainties are quoted at 1-sigma.
***Standard 2σ uncertainties of ±1.5% for $^{87}Rb/^{86}Sr$ and ±0.005% for $^{87}Sr/^{86}Sr$ are assigned to the reported isotope ratios. See Electronic Supplement for discussion.
[a] Isochron Model 1 ages were calculated with Isoplot (Ludwig, 2000) using a decay constant of $1.402*10^{-11}$ a^{-1} for ^{87}Rb (Minster et al., 1982).

as the sole carbonate mineral were identified (e.g., 488534 and 488565, respectively). Bulk-rock chemical analyses of the Tikiusaaq carbonatites (Steenfelt et al., 2007) show that calcite and dolomite carbonatites correspond to calcio- and magnesiocarbonatites, respectively, following the scheme devised by Woolley and Kempe (1989) and modified by Gittins and Harmer (1997). This geochemical terminology is used throughout the paper for the sake of consistency with forthcoming papers on the geochemistry of the Tikiusaaq intrusion.

The most abundant non-carbonate minerals of the Tikiusaaq carbonatite sheets are phlogopite, apatite, and magnetite reaching grain sizes of several mm. Fe-sulphides, predominantly pyrrhotite, are common accessory mineral phases. Euhedral amphibole, ilmenite, zircon, baddeleyite, and pyrochlore of highly variable grain size (few μm up to several mm) were identified in a small number of samples only. Olivine microphenocrysts with apatite inclusions were found in calciocarbonatite 488513.

3.1.2. Carbonatite dykes

Carbonatite dykes typically less than 0.5 m wide occur in up to 5-to-10 km distance from the carbonatite centre (Fig. 1c). Here, the country rocks show some prominent carbonate veining and coating of yellowish–reddish colour along irregular fracture patterns. The carbonatite dyke rocks are fine-grained and may contain varying proportions of euhedral to subhedral phlogopite, amphibole, clinopyroxene, olivine, and apatite microphenocrysts set in an equigranular carbonate matrix (Fig. 2b). Fe-rich dolomite and calcite are the predominant groundmass minerals, whereas Ti-magnetite, Cr-spinel, ilmenite, and rutile are relatively rare. The majority of the carbonatite dykes carry abundant country rock amphibolite and gneiss fragments. Furthermore, angular to subrounded feldspar and quartz xenocrysts are scattered throughout the carbonate-dominated matrix suggesting a violent emplacement mechanism.

3.1.3. Aillikite dykes

Carbonate-rich UML dykes typically less than 1.0 m wide occur 5-to-10 km north and east of the carbonatite centre (Fig. 1c). They occupy brittle fractures and classify as monticellite aillikites following the revised IUGS scheme of Tappe et al. (2005). Aillikite dykes have microporphyritic textures (Fig. 2c–d); however, scant olivine, phlogopite, Ti-magnetite, and ilmenite macrocrysts up to 10 mm in size, as well as rare relatively small garnet peridotite xenoliths do occur. Olivine and phlogopite form microphenocrysts set in a matrix that is composed of primary calcite, monticellite (or clinopyroxene), phlogopite, Cr-spinel, Ti-magnetite, ilmenite, and perovskite (Fig. 2c–d). Primary Ti-rich garnets with elevated Zr contents have been identified in the groundmass of a few aillikite samples. These kimzeyitic garnets are diagnostic of carbonatite–UML associations and are not known from kimberlites (Rock, 1986; Mitchell, 1995; Tappe et al., 2005).

3.2. Timing of magma emplacement

The U–Pb and Rb–Sr age results for the newly discovered Tikiusaaq carbonatite intrusion are reported in Tables 2 and 3 and summarized in Fig. 3. U–Pb concordia diagrams and two Rb–Sr isochrons are shown in Figs. 4 and 5, respectively. Descriptions of the analytical techniques and a sample list are available online as Electronic Annexes 1 and 2, respectively. Note that the U–Pb zircon age for carbonatite dyke 493310 is cited in Steenfelt et al. (2006, 2007) but no data have been previously reported. Uncertainties are quoted at the 2-sigma level throughout the text.

Table 3
Laser ablation MC-ICP-MS U–Pb zircon and baddeleyite results for Tikiusaaq carbonatites, North Atlantic craton, West Greenland.

Description*	$^{206}Pb/^{204}Pb$	$^{207}Pb/^{206}Pb$	2σ±	$^{207}Pb/^{235}U$	2σ±	$^{206}Pb/^{238}U$	2σ±	Rho	Apparent ages (Ma)				
									$^{207}Pb/^{206}Pb$	2σ±	$^{206}Pb/^{238}U$	2σ±	Discordance [%]
Calciocarbonatite sheet 488511													
1. Zrn-1 (160)	Infinite	0.04913	0.00018	0.16270	0.00125	0.02372	0.00016	0.940	154	25	151.1	4.6	2.0
1. Zrn-2 (160)	Infinite	0.04923	0.00014	0.16047	0.00084	0.02336	0.00010	0.942	159	24	148.9	4.5	6.4
1. Zrn-3 (160)	Infinite	0.04931	0.00012	0.16106	0.00146	0.02338	0.00021	0.946	163	24	149.0	4.7	8.4
1. Zrn-4 (160)	9382	0.04841	0.00165	0.15965	0.00549	0.02360	0.00009	0.626	120	84	150.3	4.5	−25.7
1. Zrn-5 (160)	20413	0.04826	0.00076	0.16364	0.00276	0.02430	0.00014	0.840	112	44	154.8	4.7	−38.0
1. Zrn-6 (160)	16185	0.04875	0.00096	0.16794	0.00340	0.02468	0.00011	0.792	136	52	157.2	4.8	−15.7
1. Zrn-7 (160)	13259	0.04895	0.00117	0.16497	0.00405	0.02419	0.00013	0.744	146	61	154.1	4.7	−5.9
1. Zrn-8 (160)	16834	0.04888	0.00092	0.16520	0.00318	0.02425	0.00009	0.801	142	50	154.4	4.7	−8.6
1. Zrn-9 (160)	infinite	0.04887	0.00020	0.16007	0.00111	0.02346	0.00013	0.937	142	25	149.5	4.6	−5.6
										WA 152.1 ± 2.3 (2σ)			
Calciocarbonatite sheet 488516													
11. Bdl-1 (12×30)	457	0.04896	0.00868	0.16532	0.03383	0.02410	0.00247	0.513	146	416	153.5	16.4	−5.1
13. Bdl-1 (12×30)	1340	0.04931	0.00396	0.15577	0.01886	0.02427	0.00220	0.761	162	189	154.6	14.8	4.8
15. Bdl-1 (12×30)	1922	0.04960	0.00480	0.16371	0.01779	0.02422	0.00119	0.504	176	227	154.3	8.9	12.4
										WA 154.2 ± 6.8 (2σ)			
Carbonatite dyke 493310													
1. Zrn-4 (160)	Infinite	0.04956	0.00150	0.16601	0.00643	0.02429	0.00059	0.762	174	70	154.7	3.8	−0.8
1. Zrn-5 (160)	1983	0.04956	0.00190	0.16583	0.00746	0.02427	0.00057	0.681	174	89	154.6	3.6	−0.8
1. Zrn-6 (160)	7862	0.04897	0.00173	0.16232	0.00704	0.02404	0.00060	0.717	146	83	153.1	3.8	0.3
1. Zrn-7 (160)	1371	0.04893	0.00178	0.16566	0.00717	0.02456	0.00057	0.697	144	85	156.4	3.7	0.5
1. Zrn-8 (160)	3685	0.04842	0.00190	0.16606	0.00750	0.02487	0.00056	0.667	120	92	158.4	3.6	1.5
1. Zrn-9 (160)	3312	0.04975	0.00221	0.17554	0.00883	0.02559	0.00061	0.630	183	103	162.9	3.9	−0.8
1. Zrn-13 (160)	5226	0.05011	0.00194	0.17291	0.00782	0.02503	0.00058	0.675	200	90	159.4	3.7	−1.6
1. Zrn-14 (160)	Infinite	0.05034	0.00183	0.17228	0.00750	0.02482	0.00059	0.701	211	84	158.0	3.8	−2.1
1. Zrn-15 (160)	32167	0.04977	0.00211	0.17624	0.00854	0.02568	0.00061	0.646	184	99	163.5	3.9	−0.8
										WA 157.8 ± 2.7 (2σ)			

*Zrn — zircon, bdl — baddeleyite; numbers in parentheses are laser spot or raster size in μm of individual analyses.
WA — weighted average $^{206}Pb/^{238}U$ dates best interpreted as carbonatite magma emplacement ages.
Note that baddeleyite fractions from calciocarbonatite sample 488516 have also been analyzed by ID–TIMS (see Table 2).
The analytical protocols employed during this study are published in Simonetti et al. (2005, 2006) and Frei and Gerdes (2009).

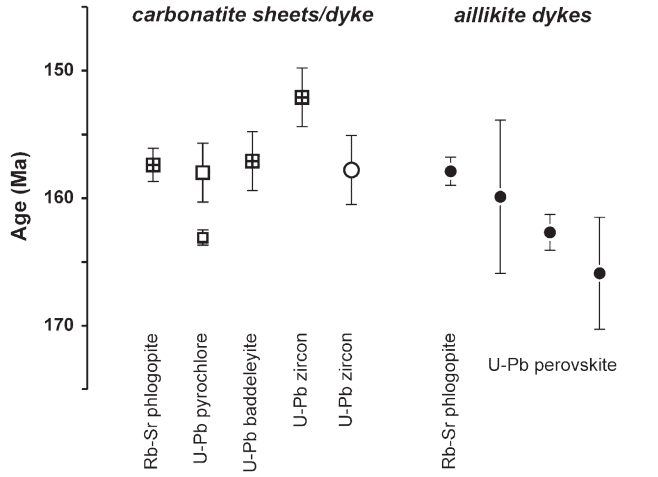

Fig. 3. Summary of the age determinations for the Tikiusaaq carbonatite sheets/dyke and aillikite dykes obtained during this study. Error bars correspond to 2-sigma uncertainties. Symbols for the different carbonatite varieties are as follows: open square with cross-hair — calciocarbonatite sheets; open square — magnesiocarbonatite sheets; open circle — *carbonatite dyke*.

Four individual *massive carbonatite sheets* that represent all parts of the 2 × 3 km large Tikiusaaq carbonatite centre were included into our geochronology study (Fig. 1c). An euhedral mm-sized zircon from calciocarbonatite sheet 488511 analyzed in-situ from a petrographic thin section by LA-MC-ICP-MS yielded a weighted average $^{206}Pb/^{238}U$ age of 152.1 ± 2.3 Ma ($n = 9$). However, it seems likely that this highly porous zircon has lost some Pb and, thus, yields an age that is slightly too young (see below). Baddeleyite identified in calciocarbonatite sheet 488516 was analyzed by two U–Pb techniques. A weighted average $^{206}Pb/^{238}U$ age of 154.2 ± 6.8 Ma was obtained by LA-MC-ICP-MS, based on three individual crystals (<30 μm) that were secured in an epoxy mount. Two multi-grain baddeleyite fractions were analyzed by ID–TIMS and yielded identical $^{206}Pb/^{238}U$ ages of 157.1 ± 2.6 Ma (fraction 1) and 157.0 ± 5.8 Ma (fraction 2). Together these two analyses yield a weighted average $^{206}Pb/^{238}U$ age of 157.1 ± 2.3 Ma. The U–Pb baddeleyite ages obtained by both techniques yield similar ages within analytical uncertainty. Two translucent yellow-to-orange octahedral pyrochlore fractions from magnesiocarbonatite sheet 488523 analyzed by ID–TIMS yielded similar $^{206}Pb/^{238}U$ ages of 157.3 ± 0.6 Ma (fraction 1) and 158.8 ± 0.8 Ma (fraction 2), which enabled calculation of a weighted average $^{206}Pb/^{238}U$ age of 158.0 ± 2.3 Ma. A third pyrochlore fraction collected from the same magnesiocarbonatite sample consisted of translucent reddish octahedrons and yielded an older $^{206}Pb/^{238}U$ age of 163.1 ± 0.6 Ma. This age is identical to a $^{206}Pb/^{238}U$ pyrochlore age of 163.5 ± 2.6 Ma for the nearby Qaqarssuk carbonatite intrusion (sample 257938; Secher et al., this issue) and is therefore best interpreted as inherited from slightly older carbonatite material that seems to be currently unexposed in the Tikiusaaq area. A four-point Rb–Sr isochron for calciocarbonatite sheet 459126 that includes three phlogopite phenocrysts and the bulk-rock carbonatite material defines an age of 157.4 ± 1.3 Ma.

A euhedral zircon macrocryst from *carbonatite dyke* 493310 (5 km to the west of the carbonatite centre) analyzed in-situ by LA-SF-ICP-MS yielded a weighted average $^{206}Pb/^{238}U$ age of 157.8 ± 2.7 Ma ($n = 9$). This age is clearly older than the U–Pb zircon age determined for calciocarbonatite sheet 488511 (152.1 ± 2.3 Ma), but identical to the U–Pb baddeleyite and pyrochlore, as well as the Rb–Sr phlogopite ages obtained for other carbonatite sheets from the carbonatite centre. These available age data suggest that carbonatite magmatism in the Tikiusaaq area occurred between ca. 164 and 155 Ma but the main magmatic pulse is much shorter-lived between ca. 158 and 155 Ma.

U–Pb perovskite ages were determined for three individual Tikiusaaq *aillikite dykes* ca. 10 km to the north and east of the carbonatite centre. In general, the U contents (45–214 ppm) and Th/U ratios (1.2–9.3) of perovskite isolated from these aillikite dykes are similar to perovskite from eastern Canadian aillikites and kimberlites (Heaman and Kjarsgaard, 2000; Tappe et al., 2006; Tappe et al., 2008a). A multi-grain perovskite fraction from aillikite dyke 488520 yielded a $^{206}Pb/^{238}U$ age of 159.9 ± 6.0 Ma. Two multi-grain perovskite fractions from aillikite 488546 yielded similar $^{206}Pb/^{238}U$ ages of 161.6 ± 2.0 Ma (fraction 1) and 163.8 ± 2.0 Ma (fraction 2), which allowed calculation

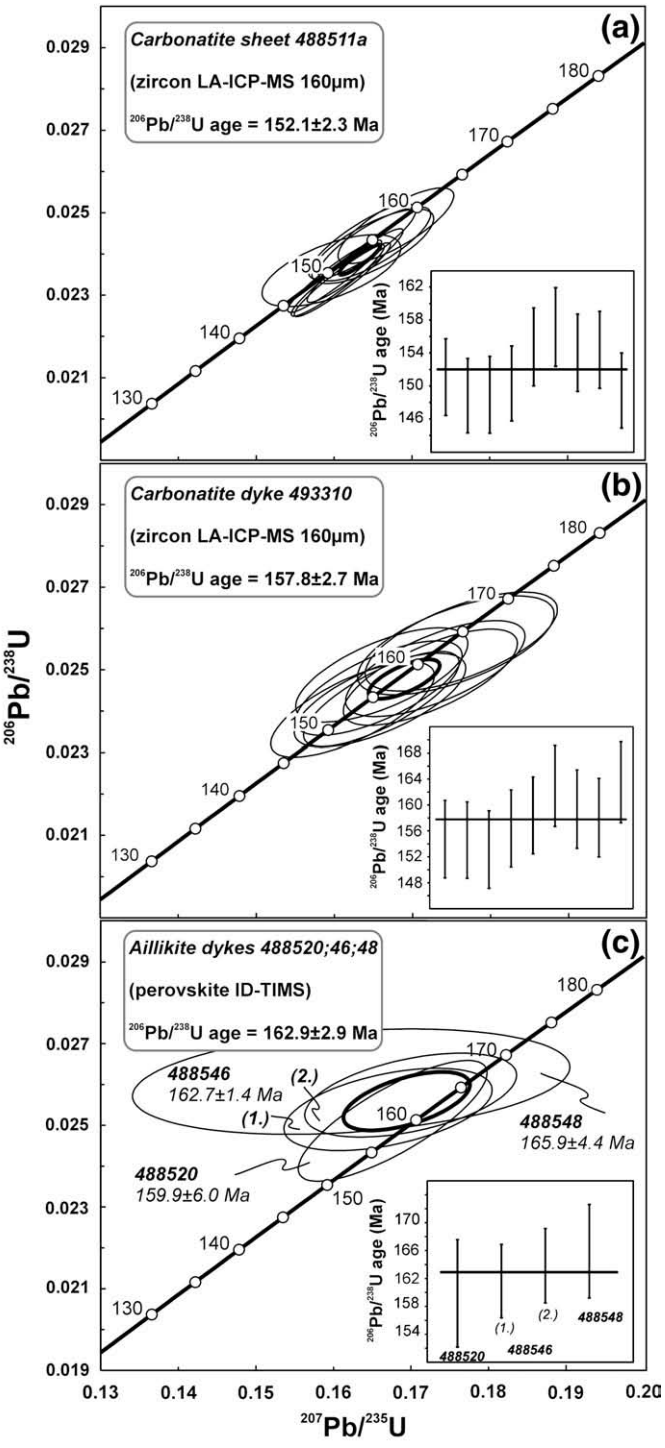

Fig. 4. Concordia diagrams displaying the results for U–Pb zircon analyses of (a) carbonatite sheet 488511a and (b) carbonatite dyke 493310, as well as U–Pb perovskite analyses of (c) aillikite dykes 488520, 488546, and 488548 from the Tikiusaaq area, West Greenland. Reported ages are $^{206}Pb/^{238}U$ dates with quoted uncertainties and envelopes at 2σ. See text and Tables 2 and 3 for further details.

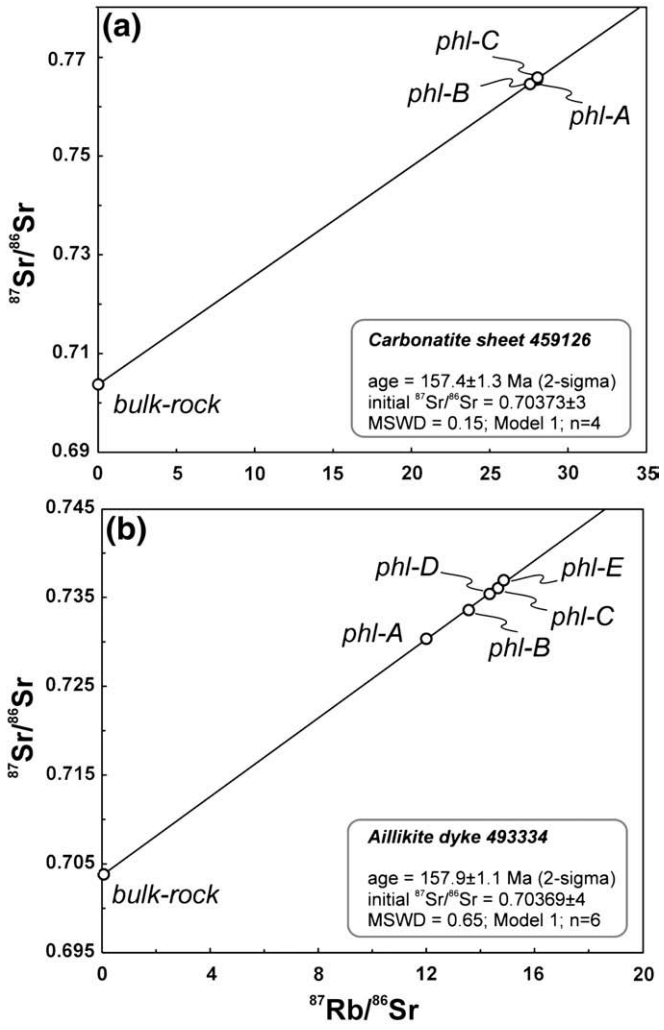

Fig. 5. Rb–Sr isochron diagrams displaying the age results for (a) carbonatite sheet 459126 and (b) aillikite dyke 493334 (quoted error and error envelopes at 2-sigma). (a) Three phlogopite phenocrysts and the host carbonatite material are included in the regression, which yields an emplacement age of 157.4 ± 1.3 Ma. (b) Five phlogopite phenocrysts and the host aillikite material are included in the regression, which yields a dyke emplacement age of 157.9 ± 1.1 Ma. A ^{87}Rb decay constant of 1.402×10^{-11} y^{-1} has been used for the age calculation following the recommendations of Amelin & Zaitsev (2002). See Table 2 and analytical techniques section in Electronic Annex 1 for further details and discussion.

of a weighted average ^{206}Pb/^{238}U age of 162.7 ± 1.4 Ma for this dyke. A ^{206}Pb/^{238}U age of 165.9 ± 4.4 Ma was determined for aillikite dyke 488548. A six-point Rb–Sr isochron for aillikite dyke 493334 that includes five phlogopite macrocrysts and the bulk-rock aillikite material suggests an emplacement age of 157.9 ± 1.1 Ma. Unfortunately, there exists no U–Pb perovskite age for aillikite dyke 493334 that would allow for a direct age comparison between the Rb–Sr and U–Pb method. However, this Rb–Sr age falls within the uncertainty limit of the U–Pb perovskite age for aillikite dyke 488520. The available age data therefore suggest that aillikite magmatism occurred between ca. 166 and 157 Ma and, thus, was coeval with the emplacement of carbonatite sheets and dykes in the Tikiusaaq area (ca. 164–155 Ma; Fig. 3).

3.3. Mineral compositions

Representative mineral chemistry data are listed in Tables 4 and 5 and the complete dataset is available online (Electronic Annexes 3–11).

3.3.1. Olivine

Olivine microphenocrysts were found in only one *carbonatite sheet* (488513) and exhibit a relatively narrow range in forsterite component ($Fo_{87–88}$ mol%; Fig. 6a), as well as CaO and MnO contents (<0.01–0.11 and 0.39–0.46 wt.%, respectively). The NiO content is below the detection limit of the electron microprobe technique (<0.02 wt.%). Olivine microphenocrysts of *carbonatite dyke 488570b* have elevated forsterite and NiO contents in the core (Fo_{87} mol%; NiO = 0.23–0.33 wt.%), but show a marked decrease toward the rim ($Fo_{82–84}$ mol%; NiO = 0.04–0.08 wt.%). Overall they fall within the compositional range of their Tikiusaaq aillikite analogues (Fig. 6a).

Euhedral to subhedral *aillikite* olivine phenocrysts/microphenocrysts exhibit a fairly large range in forsterite component ($Fo_{90–76}$ mol%), as well as NiO (<0.02–0.45 wt.%), CaO (<0.01–1.00 wt.%), and MnO (0.07–0.7 wt.%) contents. They typically show normal zoning with core compositions of $Fo_{85–90}$, decreasing to $Fo_{76–85}$ toward the rim; NiO decreases, whereas CaO and MnO typically increase. Reverse zoning in terms of Mg/Fe evolutionary trends may occur but the rim compositions of these crystals are strongly CaO-enriched (up to 1.0 wt.%). There is an anhedral to subhedral olivine population that exceeds 90 mol% forsterite (up to Fo_{93}) at constantly high NiO (0.3–0.4 wt.%; Fig. 6a) but with depleted CaO and MnO contents (<0.15 wt.%). This population overlaps the olivine compositions of cratonic spinel and garnet peridotite xenoliths from West and East Greenland (Garrit et al., 1996; Bernstein et al., 1998; Bizzarro and Stevenson, 2003; Bernstein et al., 2006) (Fig. 6a).

In general, the mode of occurrence and composition of olivine in Tikiusaaq aillikites show a strong resemblance to their analogues from the type locality at Aillik Bay in Labrador (Fig. 6a). Aillikite olivine phenocrysts/microphenocrysts are less primitive (<Fo_{90}) than those found in kimberlites and lamproites, which typically approach Fo_{93} and are not reported as having <Fo_{82} (Mitchell, 1986; Mitchell and Bergman, 1991; Fedortchouk and Canil, 2004; Prelevic et al., 2005).

3.3.2. Monticellite and clinopyroxene

Monticellite from the Tikiusaaq *aillikites* compositionally resembles its analogues from alnöites and hypabyssal kimberlites. The Ca/(Ca + Mg) ratios range between 0.50 and 0.55 similar to groundmass monticellite from Lac de Gras and Churchill kimberlites, Canada (Armstrong et al., 2004; Zurevinski et al., 2008). Although the individual monticellite crystals from the Tikiusaaq aillikites are virtually unzoned, the sample suite investigated shows a wide range of FeO (4.2–11.2 wt.%) that covers a great part of the range reported for worldwide kimberlite monticellite (Mitchell, 1986; Armstrong et al., 2004; Zurevinski et al., 2008). The MnO content approaches 0.75 wt.% comparable to kimberlitic compositions. It is, however, much lower than in the manganoan monticellite reported from a variety of carbonatites, such as the Oka complex in Quebec (Mitchell, unpublished), and the Oldoinyo Lengai and Kerimasi volcanoes in East Africa (Peterson, 1990; Church and Jones, 1995; Mitchell and Belton, 2004).

A few Tikiusaaq aillikite dykes are devoid of monticellite and contain groundmass diopside-rich clinopyroxene instead. Sample 459144 is exceptional in containing clinopyroxene that forms rims upon monticellite. This indicates groundmass crystallization close to, and across, the monticellite-diopside silica activity buffer reaction curve (Nicholls et al., 1971). Clinopyroxene overgrowths and slender prisms typically have slightly elevated Al_2O_3 and TiO_2 contents; the prisms showing subtle rimward enrichment (up to 3 wt.% Al_2O_3 and 2 wt.% TiO_2). *Carbonatite dyke* 488571 contains sparse diopside-rich clinopyroxene microphenocrysts that also show Al_2O_3 and TiO_2 enrichment toward the rim (up to 3.6 wt.% Al_2O_3 and 2.0 wt.% TiO_2). Cr_2O_3 concentrations in all these diopsides are below 0.1 wt.%. Although the Al- and Ti-enrichment in Tikiusaaq clinopyroxene is not as strong as in clinopyroxene from their Aillik Bay analogues in Labrador, the enrichment trend observed clearly goes beyond the rather restricted diopside-rich compositions reported for typical

Table 4
Representative olivine, monticellite, clinopyroxene, and phlogopite compositions from the Tikiusaaq intrusion, North Atlantic craton, West Greenland.

	Olivine										
	Carbonatite sheet				Carbonatite dyke				Aillikite dyke		
	488513	488513	488513	488513	488570b	488570b	488570b	488570b	488522	488522	488522
	pc2	pc2	pc2	pc2	pc2	pc2	pc2	pc2	mpc1	mpc1	mpc1
	core1	core2	core3	rim	core1	core2	rim1	rim2	core1	core2	rim
SiO_2	40.0	40.1	40.1	39.6	39.9	40.1	39.3	39.3	40.5	40.7	40.3
TiO_2	0.01	0.00	0.00	0.01	0.05	0.04	0.06	0.03	0.02	0.00	0.04
Al_2O_3	0.01	0.01	0.00	0.01	0.02	0.03	0.02	0.02	0.02	0.02	0.02
Cr_2O_3	0.00	0.00	0.00	0.01	0.05	0.03	0.03	0.02	0.04	0.04	0.04
FeO	11.9	11.6	12.1	11.9	12.9	13.0	15.0	14.9	8.6	8.9	13.3
MnO	0.44	0.46	0.46	0.43	0.18	0.20	0.27	0.28	0.13	0.13	0.21
NiO	0.00	0.00	0.01	0.00	0.23	0.29	0.06	0.07	0.32	0.33	0.23
MgO	47.9	48.0	47.6	47.2	46.4	46.6	44.6	44.7	50.0	49.7	46.5
CaO	0.02	0.02	0.03	0.07	0.14	0.13	0.25	0.24	0.06	0.06	0.26
Na_2O	0.00	0.00	0.00	0.01	0.05	0.04	0.02	0.12	0.02	0.00	0.03
K_2O	0.00	0.00	0.00	0.00	0.01	0.00	0.00	0.01	0.00	0.00	0.00
Total	100.3	100.1	100.3	99.3	99.9	100.5	99.6	99.6	99.7	99.9	100.9

	Phlogopite														
	Carbonatite sheets									Carbonatite dykes					
	Phl	Phl	Phl	Phl	Phl	Phl	Phl	Phl	Phl	Phl	Phl	Phl	Phl	Phl	Phl
	488511a	488511a	488511a	488511a	488523	488523	488523	488523	488523	488568	488568	488568	488568	488568	488570b
	pc1	pc1	pc1	pc1	pc1	pc1	pc1	pc1	pc1	pc1	pc1	pc1	pc1	pc1	pc5
	core1	core2	rim1	rim2	core1	core2	core3	rim1	rim2	core1	core2	core3	rim1	rim2	core1
SiO_2	40.23	40.49	41.79	41.66	42.06	40.49	41.13	40.43	39.99	39.86	39.99	38.45	36.05	36.14	37.83
TiO_2	0.09	0.08	0.16	0.27	0.20	0.31	0.35	0.18	0.17	3.26	3.26	3.70	2.55	2.39	4.81
Al_2O_3	13.62	13.97	11.26	11.09	8.28	8.71	9.21	9.27	8.90	11.99	11.82	12.91	16.85	16.88	14.42
Cr_2O_3	0.00	0.00	0.01	0.03	0.00	0.02	0.04	0.01	0.00	0.15	0.14	0.38	0.00	0.04	0.97
FeO	4.27	4.41	7.02	7.49	11.57	14.53	10.54	13.12	13.73	7.73	7.92	6.81	6.70	6.78	6.72
MnO	0.06	0.04	0.09	0.04	0.09	0.05	0.08	0.06	0.01	0.05	0.02	0.07	0.08	0.07	0.08
MgO	25.05	25.46	24.00	23.99	22.70	21.20	22.58	21.45	21.15	20.95	21.45	21.04	21.43	21.37	20.31
CaO	0.00	0.02	0.05	0.07	0.01	0.01	0.00	0.06	0.05	0.02	0.03	0.02	0.09	0.08	0.06
BaO	0.35	0.36	0.05	0.01	0.00	0.05	0.04	0.06	0.06	0.11	0.08	0.18	1.46	1.29	0.27
Na_2O	0.33	0.34	0.36	0.34	0.41	0.18	0.40	0.18	0.29	0.40	0.48	0.45	0.52	0.51	0.43
K_2O	9.97	10.00	10.00	9.94	9.77	9.85	9.77	9.74	9.60	9.94	9.62	9.66	9.33	9.18	9.47
F	2.24	2.38	2.99	3.12	2.84	2.62	2.66	2.82	2.40	0.70	0.72	0.52	0.44	0.35	0.41
Cl	0.00	0.02	0.00	0.00	0.00	0.00	0.01	0.00	0.02	0.02	0.01	0.00	0.00	0.01	0.02
O=F	−0.94	−1.00	−1.26	−1.31	−1.20	−1.10	−1.12	−1.19	−1.01	−0.29	−0.30	−0.22	−0.18	−0.15	−0.17
Total	95.3	96.6	96.5	96.7	96.7	96.9	95.7	96.2	95.4	94.9	95.2	94.0	95.3	94.9	95.6

Pc — phenocryst; mpc — microphenocryst; gm — groundmass; Phl — phlogopite; TFP — tetraferriphlogopite.

groundmass clinopyroxene in orangeites and lamproites (Mitchell and Bergman, 1991; Mitchell, 1995).

3.3.3. Phlogopite and amphibole

Phlogopite phenocrysts from both *magnesio-* and *calciocarbonatite sheets* appear to be virtually unzoned and are Al-depleted (8–14 wt.% Al_2O_3; Fig. 7). They are generally Ti- and Ba-poor (<1.0 wt.% TiO_2 and 0.6 wt.% BaO). While magnesiocarbonatite phlogopites exhibit a wide range in FeO content (5.2–14.9 wt.%; Mg# 76–85), calciocarbonatite phlogopites are characterized by FeO contents <8 wt.% (Mg# 84–96). The 'higher FeO' magnesiocarbonatite phlogopites are exclusively F-rich (2.0–3.2 wt.% F), whereas calciocarbonatite phlogopites show a wide range in F contents (0.5–3.3 wt.% F). The *carbonatite dykes* contain abundant phlogopite phenocrysts/microphenocrysts and tiny groundmass flakes of broadly similar composition within individual samples. However, there is a wide compositional range within the carbonatite dyke suite (Fig. 7) in terms of phlogopite Al_2O_3 (5–20 wt.%), TiO_2 (0.1–5 wt.%), FeO (5–19 wt.%), and F (0.2–3.0 wt.%) concentrations. The full extent of this variation is not observed within individual samples and there is no single evolutionary trend as both rimward Al, Ti, and F enrichment and depletion occur. For example, phlogopite microphenocrysts from carbonatite dyke 488570 show discrete overgrowths that are rich in titanian tetraferriphlogopite component, indicating Al-depletion and Fe-enrichment of the residual carbonatite liquid; whereas Fe-enriched microphenocrysts of biotitic composition show phlogopite overgrowths in carbonatite dyke 488572. Phlogopite cores typically have <1.0 wt.% BaO and there is an increase toward the rim approaching 2.5 wt.% BaO. Aillikite dykes contain relatively rare phlogopite phenocrysts/microphenocrysts and more abundant tiny groundmass flakes. Some of the phenocrysts/microphenocrysts have elevated TiO_2 concentrations in the cores (2–7 wt.%) and there is an overall trend of decreasing Ti toward the rims. Although a few samples contain phenocryst and groundmass phlogopite that shows rimward Al-enrichment (i.e., up to 21 wt.% Al_2O_3; 488520; 488539; 488552), the majority of aillikite dykes are characterized by phlogopite that exhibits rimward Al-depletion (i.e., down to 10 wt.% Al_2O_3; 459144; 488527; 488549; and 488562). This trend may culminate in virtually Al- and Ti-free tetraferriphlogopite rims (Fig. 7). While tetraferriphlogopite is uncommon in kimberlites, the rims reported here are similar to those from Aillik Bay and Sarfartoq aillikites. Phlogopite from the Tikiusaaq aillikite dykes is Ba-poor with core compositions typically <1.5 wt.% BaO. Rim compositions may approach 3.5 wt.% BaO, which is slightly higher if compared to Aillik Bay and Sarfartoq phlogopite phenocrysts (typically <2.0 wt.% BaO). The F content is highly variable ranging between 0.2 and 2.0 wt.% similar to the range reported for phlogopite from Aillik Bay aillikites and carbonatites. The Tikiusaaq aillikite phlogopite compositional spectrum is clearly distinct from groundmass phlogopite in kimberlite, which typically shows a strong Al- and Ba-enrichment and Ti-depletion toward the rim.

In summary, phlogopite phenocrysts/microphenocrysts from the Tikiusaaq aillikite and carbonatite dykes exhibit a wide Al and Ti

Monticellite					Clinopyroxene					
Aillikite dykes					Carbonatite dyke			Aillikite dyke		
488520	488520	488538	488538	488538	488571	488571	488571	488549b	488549b	488549b
gm2	gm2	gm4	gm4	gm4	pc3	pc3	pc3	gm1	gm1	gm1
core	rim	core	rim1	rim2	core1	core2	rim	core	rim1	rim2
37.0	37.0	36.9	37.0	37.0	53.3	49.8	53.2	51.6	50.8	52.0
0.05	0.04	0.12	0.06	0.08	0.10	1.67	0.09	0.76	1.01	0.67
0.03	0.01	0.02	0.02	0.01	1.45	2.79	1.45	1.43	2.30	1.30
0.00	0.00	0.00	0.01	0.00	0.00	0.00	0.02	0.00	0.02	0.00
8.08	7.88	8.21	7.59	7.39	7.05	5.10	7.10	4.61	4.95	4.25
0.51	0.54	0.69	0.62	0.52	0.34	0.14	0.33	0.16	0.10	0.18
0.02	0.01	0.01	0.01	0.03	0.00	0.01	0.00	0.00	0.00	0.00
21.9	21.7	21.7	21.8	21.9	13.4	14.7	13.5	15.2	14.8	15.3
31.9	32.3	32.3	32.6	32.4	23.0	24.7	22.8	25.1	25.3	25.3
0.05	0.03	0.03	0.04	0.05	1.55	0.36	1.57	0.32	0.41	0.29
0.01	0.01	0.04	0.05	0.04	0.00	0.01	0.01	0.01	0.01	0.00
99.5	99.5	100.0	99.9	99.4	100.1	99.3	100.0	99.2	99.6	99.2

				Aillikite dykes										
Phl	Phl	TFP	TFP	Phl	Phl	TFP	TFP	Phl	TFP	TFP	Phl	Phl	Phl	Phl
488570b	488570b	488570b	488570b	488527	488527	488527	488527	488562	488562	488562	488552	488552	488552	488552
pc5	pc5	pc5	pc5	mpc5	mpc5	mpc5	mpc5	mpc9	mpc9	mpc9	mpc8	mpc8	mpc8	mpc8
core2	core3	rim1	rim2	core1	core2	rim1	rim2	core	rim1	rim2	core1	core2	rim1	rim2
37.85	37.74	41.21	41.66	38.55	37.50	39.56	39.69	40.94	40.64	41.12	37.28	37.34	35.71	34.91
4.58	4.74	1.36	2.40	1.08	0.75	0.41	0.40	0.96	0.03	0.05	4.74	4.75	1.09	1.20
14.43	14.52	8.14	6.40	13.93	15.67	0.25	0.50	10.69	0.72	2.37	14.91	15.02	19.02	19.60
0.23	0.50	0.00	0.00	0.00	0.05	0.04	0.00	0.00	0.02	0.00	0.09	0.01	0.03	0.00
7.13	6.85	11.31	12.36	8.67	9.04	17.87	17.65	6.71	15.75	13.40	7.72	7.72	4.62	4.56
0.05	0.04	0.38	0.26	0.08	0.13	0.11	0.15	0.03	0.29	0.18	0.06	0.06	0.08	0.06
20.43	20.83	21.77	20.93	21.81	21.05	25.41	25.18	24.48	26.09	26.37	20.33	20.56	23.00	22.54
0.12	0.06	0.25	0.24	0.08	0.14	0.21	0.28	0.13	0.26	0.22	0.06	0.07	0.13	0.16
0.25	0.27	0.06	0.08	0.08	0.22	0.06	0.01	0.15	0.04	0.01	0.44	0.47	2.12	2.17
0.48	0.45	0.28	0.36	0.61	0.58	0.36	0.29	0.22	0.18	0.18	0.53	0.47	0.31	0.28
9.55	9.59	9.89	9.77	9.63	9.56	8.03	8.50	10.26	9.63	9.99	9.38	9.52	9.23	9.29
0.42	0.36	2.00	1.96	0.65	0.76	1.12	1.45	1.11	1.37	1.57	0.48	0.42	0.46	0.58
0.01	0.01	0.01	0.02	0.00	0.01	0.00	0.01	0.02	0.01	0.02	0.00	0.01	0.02	0.00
−0.18	−0.15	−0.84	−0.83	−0.27	−0.32	−0.47	−0.61	−0.47	−0.58	−0.66	−0.20	−0.18	−0.19	−0.24
95.4	95.8	95.8	95.6	94.9	95.1	92.9	93.5	95.2	94.5	94.8	95.8	96.2	95.6	95.1

compositional range that is broadly overlapping and bears similarity to the compositional range reported from other worldwide UML-carbonatite occurrences. In contrast, phlogopite phenocrysts from the massive Tikiusaaq carbonatite sheets exhibit a relatively narrow compositional range that is characterized by strong Al and Ti depletion (Fig. 7).

The amphibole needles identified in a few of the massive carbonatite sheets approach pure richterite end-member composition. They have high Mg# between 93 and 96. K_2O and TiO_2 are below 0.5 and 0.15 wt.%, respectively. Fluorine is slightly elevated and scatters around 1.0 wt.%. The euhedral amphibole microphenocrysts in the carbonatite dykes comprise both magnesio-arfvedsonite (sodic amphibole) and magnesiokatophorite (sodic–calcic amphibole) compositions. They show a wide range in Mg# between 60 and 85, and magnesiokatophorite forms rims upon magnesio-arfvedsonite microphenocrysts. TiO_2 is typically low and only rarely exceeds 1.0 wt.% (up to 1.3 wt.% TiO_2). K_2O varies between 0.2 and 1.8 wt.% and typically decreases rimwards. However, no systematic trend in the Na_2O core–rim evolution was recognized. Fluorine concentrations range between 0.2 and 2.5 wt.% and typically decrease toward the rims.

3.3.4. Spinel and ilmenite

The sole spinel group mineral of the Tikiusaaq *calcio- and magnesiocarbonatite sheets* is magnetite typically occurring in clusters that may align as discrete bands. Magnetite approaches end-member composition (Fe_3O_4) with important minor components such as TiO_2, Al_2O_3, Cr_2O_3, MgO, and MnO accounting for less than 3.5 wt.% of individual analyses. Primary spinel group minerals <100 μm across comprise a significant proportion of the groundmass mineral assemblage of the Tikiusaaq carbonatite and aillikite dykes. They follow a 'titanomagnetite trend' (trend 2 of Mitchell, 1986) that is characterized by $Fe_T^{2+}/(Fe_T^{2+}+Mg)>0.6$ (Fig. 6b), increasing Fe and Ti, but decreasing Mg, Al, and Cr. However, groundmass spinels from the carbonatite dykes are less magnesian (<6 wt.% MgO) if compared to their aillikite analogues (up to 14 wt.% MgO). Tikiusaaq aillikite groundmass spinel compositions are similar to their Aillik Bay and Sarfartoq analogues in terms of Fe/Mg evolution and partly fall in between the 'titanomagnetite trend' and 'magnesian ulvöspinel trend' (trend 1 of Mitchell, 1986) if projected onto the front face of the 'reduced' spinel prism (Fig. 6b). However, aillikite spinels are clearly less magnesian (4–14 wt.% MgO) relative to primary groundmass kimberlite spinels (12–25 wt.% MgO), which define the 'magnesian ulvöspinel trend' of increasing Ti at buffered Fe/Mg of between 0.4–0.6 (Mitchell, 1986). Note furthermore that spinel compositions from the extensive aillikite dyke swarms at Tikiusaaq, Sarfartoq, and Aillik Bay provide near-complete coverage of the whole evolutionary spectrum (Fig. 6b) and that there are also similarities in terms of Cr/Al evolution, i.e., Cr# (Cr/(Cr+Al)) is below 0.85 (not shown). By comparison, lamproites and orangeites typically contain Cr-richer spinel that is strongly depleted in Al (Cr#>0.85) and follows the 'titanomagnetite trend' (Mitchell and Bergman, 1991; Mitchell, 1995).

Table 5
Representative spinel and Ti-rich primary groundmass garnet compositions from the Tikiusaaq intrusion, North Atlantic craton, West Greenland.

	Spinel group minerals																										
	Carbonatite sheets					Carbonatite dykes									Aillikite dykes												
	Mag	Mag	Mag	Mag	Mag	Mag	Mag	Mag	Cr-Spl	Cr-Spl	Cr-Spl	Ti-Mag	Ti-Mag	Ti-Mag	Cr-Spl	Cr-Spl	Ti-Mag	Ti-Mag	Ti-Mag	Ti-Mag	Ti-Mag	Ti-Mag	Ti-Mag	Cr-Spl	Ti-Mag	Ti-Mag
	488513	488513	488513	488523	488523	488563a	488563a	488563a	488570b	488570b	488570b	488571	488571	488571	488522	488522	488522	488522	488522	488538	488538	488538	488538	488562	488562	488562
	mpc2	mpc2	mpc2	mpc1	mpc1	mpc5	mpc5	mpc5	mpc7	mpc7	mpc7	mpc7	mpc7	mpc7	mpc8	mpc8	mpc8	mpc8	mpc8	mpc1	mpc1	mpc1	mpc1	mpc2	mpc2	mpc2
	core	rim1	rim2	core	rim	core1	core2	core3	core	rim1	rim2	core1	core2	core3	core1	core2	rim1	rim2	rim3	core1	core2	rim1	rim2	core	rim1	rim2
SiO_2	0.06	0.06	0.10	0.09	0.05	0.13	0.12	0.11	0.04	0.06	0.04	0.07	0.09	0.05	0.09	0.25	0.09	0.41	0.11	0.09	0.07	0.08	0.08	0.09	0.11	0.06
TiO_2	1.78	1.61	1.41	0.11	0.10	0.49	0.50	0.50	0.69	0.72	0.68	7.19	7.31	7.22	5.93	5.42	16.75	13.94	14.62	13.10	13.04	15.76	16.96	9.04	15.85	9.51
Al_2O_3	0.06	0.07	0.08	0.01	0.02	0.41	0.40	0.69	10.96	11.09	10.85	1.79	1.80	1.78	6.40	8.36	3.54	3.73	6.80	1.44	1.43	2.59	4.46	7.94	5.89	3.74
Cr_2O_3	0.00	0.02	0.01	0.02	0.03	0.01	0.00	0.00	41.75	40.95	41.23	0.03	0.03	0.01	37.11	40.32	4.51	12.46	2.04	1.96	1.86	0.87	0.62	31.37	3.93	0.05
V_2O_3	0.19	0.18	0.23	0.22	0.23	0.06	0.05	0.06	0.15	0.16	0.17	0.22	0.19	0.21	0.17	0.23	0.26	0.25	0.17	0.49	0.46	0.40	0.22	0.23	0.23	0.25
FeO[a]	91.11	91.23	91.48	93.49	93.57	91.68	91.89	91.82	42.42	42.43	42.38	81.52	81.22	81.40	40.23	35.90	61.33	56.68	62.01	72.54	73.45	69.19	65.54	38.34	60.06	74.35
MnO	0.39	0.37	0.22	0.04	0.04	0.38	0.37	0.39	0.97	0.97	0.95	0.55	0.54	0.54	0.68	0.61	0.72	0.72	0.72	0.58	0.53	0.65	0.68	0.78	0.94	0.81
NiO	0.00	0.01	0.02	0.01	0.00	0.00	0.00	0.02	0.04	0.05	0.06	0.01	0.00	0.01	0.18	0.14	0.16	0.22	0.08	0.05	0.06	0.03	0.05	0.11	0.06	0.03
MgO	1.28	1.34	0.89	0.01	0.03	0.48	0.41	0.46	3.31	3.40	3.19	4.69	4.75	4.47	9.69	9.59	11.02	10.56	11.92	7.03	6.52	7.94	9.22	12.61	11.71	7.62
Total	94.86	94.89	94.43	94.00	94.07	93.64	93.74	94.03	100.34	99.82	99.55	96.06	95.92	95.68	100.48	100.82	98.38	98.97	98.47	97.28	97.43	97.51	97.83	100.51	98.78	96.43

	Ti-rich primary garnets																
	Aillikite dykes																
	Kim	Kim	Kim	Kim	Kim	Kim	Kim	Kim	Kim	Kim	Kim	Kim	Kim	Kim	Kim	Kim	Kim
	459144	459144	459144	459144	459144	459144	459144	459144	459142	459142	459142	459142	459142	459142	459142	459142	459142
	gm1	gm1	gm1	gm1	gm1	gm12	gm12	gm12	gm2	gm2	gm2	gm8	gm8	gm8	gm10	gm10	
	core1	core2	rim1	rim2	rim3	core1	core2	rim	core1	core2	rim	core1	core2	rim	core1	core2	
SiO_2	25.00	24.16	24.08	24.01	24.63	25.97	26.29	25.75	20.67	20.55	20.70	20.43	20.67	20.09	19.14	18.32	
TiO_2	10.80	10.58	10.46	11.24	10.84	10.87	10.91	10.83	10.16	10.26	10.19	10.26	10.27	10.41	14.32	10.61	
ZrO_2	15.59	16.99	16.90	16.01	16.01	14.69	14.45	14.77	19.97	20.13	19.84	20.56	20.44	20.75	18.92	22.25	
HfO_2	0.33	0.30	0.27	0.32	0.35	0.31	0.31	0.30	0.39	0.39	0.42	0.38	0.38	0.37	0.42	0.36	
Al_2O_3	1.08	1.43	1.58	1.13	1.04	0.76	0.73	0.78	3.79	3.82	3.75	3.76	3.79	3.94	3.68	4.44	
FeO[a]	13.88	13.51	13.62	14.10	13.87	14.07	14.07	14.23	11.89	11.88	11.99	11.98	12.24	12.24	11.23	12.27	
MnO	0.17	0.14	0.14	0.19	0.19	0.21	0.21	0.20	0.11	0.11	0.09	0.08	0.08	0.08	0.08	0.07	
MgO	2.95	2.85	2.83	2.72	2.92	3.01	3.04	2.99	2.46	2.38	2.42	2.26	2.36	2.21	2.20	1.75	
CaO	30.36	30.50	30.56	30.48	30.47	30.59	30.77	30.68	30.44	30.19	30.21	29.97	30.15	30.27	31.18	30.10	
Na_2O	0.32	0.23	0.17	0.24	0.32	0.26	0.25	0.31	0.08	0.05	0.06	0.09	0.06	0.12	0.13	0.08	
Total	100.5	100.7	100.6	100.4	100.6	100.7	101.0	100.8	100.0	99.8	99.7	99.8	100.4	100.5	101.3	100.2	

Cr-Spl — chromian spinel; Ti-Mag — titanomagnetite; Mag — magnetite; Kim — kimzeyite-rich Ti-andradite garnet; mpc — microphenocryst; gm — groundmass.
[a] FeO as total Fe.

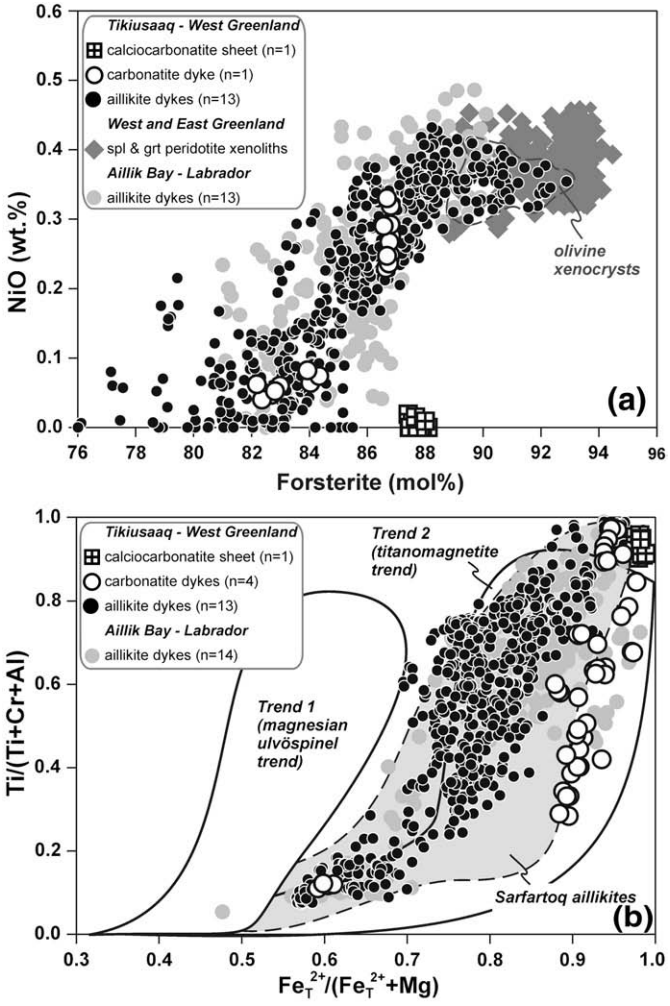

Fig. 6. (a) NiO (wt.%) vs. forsterite (mol%) variation in olivine phenocrysts/microphenocrysts in carbonatite sheet 488513 and carbonatite dyke 488570, as well as in various aillikite dykes from the Tikiusaaq intrusion, West Greenland. Note the similar olivine compositional trends of the Tikiusaaq aillikites and the type rocks from Aillik Bay in Labrador (Tappe et al., 2006). The outline indicates an olivine population that is interpreted as xenocrystic mantle-derived. Olivine data for spinel and garnet peridotite xenoliths from West (Ubekendt Island and Sarfartoq–Maniitsoq areas) and East Greenland (Wiedemann Fjord) are shown for comparison (Garrit et al., 1996; Bernstein et al., 1998; Bizzarro and Stevenson, 2003; Nielsen and Sand, 2008; and unpublished data of Stefan Bernstein). (b) Atomic Ti/(Ti + Cr + Al) vs. $Fe_T^{2+}/(Fe_T^{2+}+Mg)$ for spinels in a carbonatite sheet, carbonatite dykes, and aillikite dykes from the Tikiusaaq intrusion. Spinels in Tikiusaaq aillikite dykes follow magmatic trend 2 ("titanomagnetite trend") in contrast to kimberlite spinel compositions, which are rich in magnesian ulvöspinel component (magmatic trend 1 of Mitchell, 1986). Aillik Bay (Tappe et al., 2006) and Sarfartoq data (courtesy of Troels Nielsen) are shown for comparison.

Chromite-spinel solid solutions with up to 43 wt.% Cr_2O_3, 10 wt.% Al_2O_3, and 13 wt.% MgO rarely occur as inclusions in olivine microphenocrysts (e.g., aillikite dyke 488538). These Cr-spinel inclusions are compositionally similar to early-stage Cr-spinel microphenocrysts set in the aillikite groundmass (up to 46 wt.% Cr_2O_3), which bear striking resemblance to Cr-spinel microphenocrysts in type aillikites from Aillik Bay except for the slightly elevated Al_2O_3 contents of the latter (up to 12 wt.% Al_2O_3). Composite spinel grains from Tikiusaaq aillikites may contain cores of titanian magnesiochromite-chromite solid solution (up to 15 wt.% TiO_2, 14 wt.% MgO, and 28 wt.% Cr_2O_3). Rims of these zoned spinel microphenocrysts and individual groundmass grains are of ulvöspinel-magnesian ulvöspinel–magnetite composition (up to 14 wt.% MgO). These titanomagnetites are enriched in Al_2O_3 (up to 12 wt.%) with low Cr# of <0.3. Titanomagnetite to magnetite macrocrysts up to 5 mm across are a rare but widespread constituent of the Tikiusaaq aillikites. Core compositions are strongly Al_2O_3 depleted (<5 wt.%), whereas rims may approach Al_2O_3 contents similar to groundmass titanomagnetite (up to 14 wt.%).

Ilmenite laths were found in magnesiocarbonatite sheet 488523 and are almost pure $FeTiO_3$. They are MnO and MgO poor (<0.8 and <0.2 wt.%, respectively) and devoid of Cr_2O_3 (<0.03 wt.%). Groundmass ilmenite in aillikite dykes is moderately enriched in MgO (6–10 wt.%); however, it is much less magnesian than its analogues from archetypal kimberlites (12–24 wt.%; Mitchell (1986)). Groundmass ilmenite MnO (0.4–3.0 wt.%) and Cr_2O_3 (0–3.0 wt.%) contents may be similarly elevated in both aillikite and calcite kimberlite dykes. Groundmass ilmenite was identified in Tikiusaaq carbonatite dyke 488571 and falls within the ilmenite compositional range observed for aillikites. Ilmenite macrocrysts up to 10 mm across occur in Tikiusaaq aillikites and they have much higher MgO contents (9–15 wt.%) compared to the groundmass ilmenite (6–10 wt.%). These macrocrysts show a similar range of slightly elevated Cr_2O_3 (0–3 wt.%) and MnO (0.2–1 wt.%) concentrations as the groundmass ilmenites, but their hematite component (7–12 mol%) is lower than in the groundmass ilmenites (12–18 mol%) recording less oxidizing crystallization conditions. Both the ilmenite macrocrysts and groundmass laths show titanomagnetite overgrowth that differs with respect to its Cr_2O_3 content depending on which type of ilmenite they formed on (>1.0 wt.% and <0.4 wt.%, respectively). Spinel overgrowth compositions dependent on ilmenite host have been reported from Finland aillikites and kimberlites (O'Brien and Tyni, 1999).

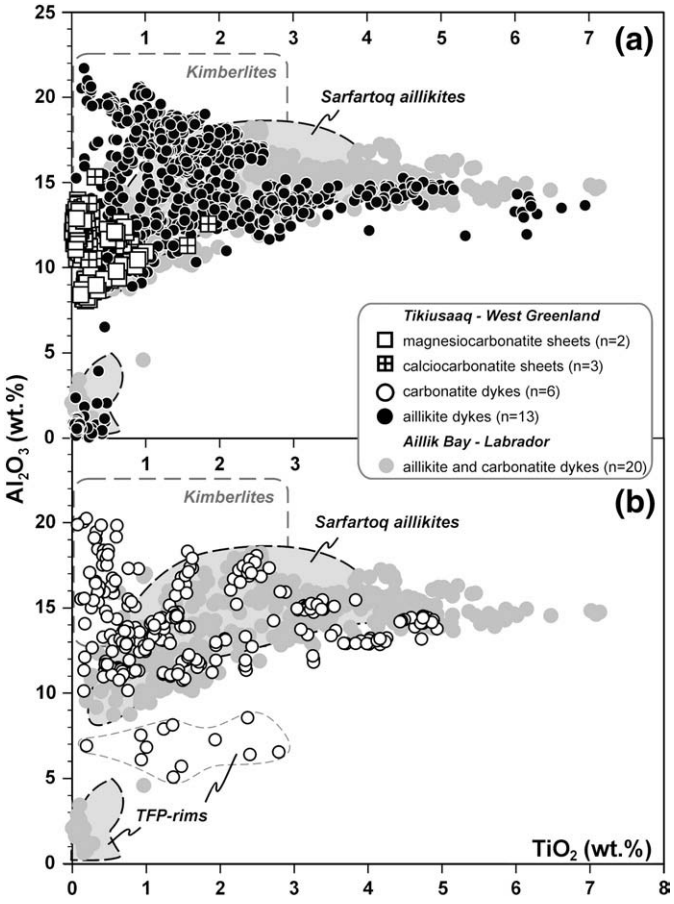

Fig. 7. Al_2O_3 vs. TiO_2 (wt.%) variation of phlogopite in (a) carbonatite sheets and aillikite dykes, and (b) carbonatite dykes from the Tikiusaaq intrusion, West Greenland. Aillik Bay (Tappe et al., 2006) and Sarfartoq data (courtesy of Troels Nielsen), as well as the 'kimberlite box' (Mitchell, 1995) are shown for comparison. TFP — tetraferriphlogopite.

3.3.5. Perovskite and Ti-rich primary garnet

Perovskite (20–200 μm) and kimzeyitic garnet (<100 μm) are restricted to the groundmass of the *aillikite dykes* in the Tikiusaaq area. Tikiusaaq perovskite, like those from type aillikites at Aillik Bay and global kimberlites, are close to the ideal $CaTiO_3$ end-member composition (cf., Mitchell, 1995; Tappe et al., 2006). However, a negative correlation between atomic Ca and Na plus LREE indicates solid-solution between perovskite and loparite ($Na_{0.5}LREE_{0.5}TiO_3$), with Na_2O and $LREE_2O_3$ commonly not exceeding 0.7 and 2.6 wt.%, respectively (note that only La_2O_3 and Ce_2O_3 were measured during this study). The SrO (0.1–0.3 wt.%) and Nb_2O_5 (0.3–1.4 wt.%) contents are slightly elevated in zoned perovskites.

Small kimzeyitic garnets (Zr-rich Ti-andradite) have a fairly constant TiO_2 content (9–12 wt.%), whereas there is significant intergrain compositional variation in terms of ZrO_2 contents (12–22 wt.%; Table 5). Core-to-rim zonation of individual garnet grains was not observed. The presence of kimzeyitic garnet reflects the high Ca but low Al concentration of the aillikite magma and is regarded diagnostic of carbonatite–UML associations (Platt and Mitchell, 1979; Rock, 1986; Tappe et al., 2005). These garnets do not occur in kimberlites and lamproites (Mitchell and Bergman, 1991; Mitchell, 1995).

3.3.6. Carbonates

Calcio- and magnesiocarbonatite sheets are composed of variable mixtures of calcite and dolomite; the compositions of the carbonate phases are broadly overlapping between rock types. Dolomite crystals of calcio- and magnesiocarbonatite contain between 1–9 wt.% and 2–7 wt.% FeO, respectively. Interestingly, dolomite of the carbonatite dykes reaches up to 14 wt.% FeO. Calcite is generally FeO-poor in all carbonatite lithologies and the aillikite dykes (<2.0 wt.%). MnO is significantly elevated in dolomite of the calciocarbonatites, whereas it is only mildly enriched in its magnesiocarbonatite counterparts (0.2–1.7 vs. 0.3–0.7 wt.% MnO, respectively). Calcite from all carbonatite lithologies contains between 0.1–0.8 wt.% MnO; groundmass calcite in aillikites typically contains less than 0.2 wt.% MnO. The SrO contents of both calcite and dolomite are highly variable and range between 0.2–2.0 wt.% for all carbonatite lithologies and the aillikite dykes.

4. Discussion

It is a "well-known fact" that there is a genetic relationship between spatially associated carbonatites and alkaline silicate rocks. The models in which these magma groups have been linked essentially consider two options: (1) an increasing degree of partial melting of carbonated peridotite, i.e., a primary melting relationship, or (2) magmatic differentiation by which carbonatite magmas evolve from parental carbonated silicate melts. However, Gittins and Harmer (2003) pointed out that spatial association does not necessarily imply a genetic relationship and that a variety of information, including age data, from individual units within a single carbonatite complex are required in order to evaluate the possible petrogenetic links.

In the following discussion we will consider the timing and style of carbonatite and aillikite magma emplacement in the Tikiusaaq area; we view the new age data within a wider tectonomagmatic framework that considers deep carbonate–potassic silicate magmatism as a consequence of incipient rifting of cratonic mantle lithosphere.

4.1. Tikiusaaq — a new carbonatite-aillikite occurrence

The mineralogical criteria discussed in detail in Section 3.3. clearly identify the Tikiusaaq carbonate-rich ultramafic potassic dykes as aillikites. They bear strong resemblance to their Sarfartoq and Aillik Bay counterparts. These rocks differ in important mineralogical aspects from petrographically similar archetypal kimberlites (Mitchell et al., 1999; Tappe et al., 2005; Tappe et al., 2006), that is, they are derived from different parental magmas. The presence of abundant primary groundmass carbonate in the aillikite dykes (Fig. 2c–d) that occur in the vicinity of the massive carbonatite sheets at Tikiusaaq, along with their overlapping emplacement ages (Fig. 3), point to a petrogenetic relationship between these rock types. The aillikite dykes occupy well-defined brittle fractures and show signs of rapid solidification; whereas multiple pulses of carbonatite magma were emplaced into a ductile shear zone where they cooled slowly as sheet intrusions causing intense wall-rock alteration. This mode of occurrence observed at Tikiusaaq is virtually identical to the emplacement features recognized at Sarfartoq (Secher and Larsen, 1980) and Qaqarssuk (Knudsen and Buchardt, 1991) and suggests that the carbonatite sheets are differentiation products presumably derived from the carbonate-rich aillikite magma. Geochemical data, including stable and radiogenic isotope compositions, and mass balance considerations support this hypothesis (Tappe et al., 2008b), and they will be discussed in detail elsewhere. We now discuss the tectonic significance of this deep carbonate–potassic silicate magmatism.

4.2. Tectonic significance of carbonatite-aillikite magmatism

The new U–Pb and Rb–Sr age determinations reported here for a variety of primary minerals suggest that carbonatite and aillikite magmatism at Tikiusaaq was broadly coeval and occurred between ca. 165 and 155 Ma (Fig. 3). Several other Jurassic carbonatite and aillikite occurrences in close proximity to Tikiusaaq are known from the Maniitsoq area 150 km to the north (Qaqarssuk), the Faeringehavn area 100 km to the southwest, and the Frederikshåb Isblink area 150 km to the south (Fig. 1b). Bizzarro et al. (2002), Larsen (2006), and Secher et al. (this issue) reported U–Pb and Rb–Sr age data for the timing of carbonatite-aillikite magmatism at Qaqarssuk (aillikite 'explosion' breccia, 164.2 ± 1.8 Ma; aillikite dyke, 165.7 ± 1.2 Ma; carbonatite sheets, 164 ± 5 Ma, 163.5 ± 2.6 Ma, and 165.0 ± 0.9 Ma) and Frederikshåb Isblink (alnöite dyke, 152.1 ± 3.2 Ma) suggesting it was contemporaneous with magmatism at Tikiusaaq. Note that K–Ar phlogopite analyses of the aillikite and carbonatite dykes in the Faeringehavn area also yielded Mesozoic ages (196–175 Ma; Larsen and Rex, 1992), but the quality of these age results is considered poor (Lotte Larsen, personal communication). Further, Mesozoic aillikite and alleged kimberlite dykes have been reported from the Paamiut and Pyramidefjeld areas approximately 250 km south of Tikiusaaq in southern Greenland (Fig. 1b). The K–Ar phlogopite ages range between 220 and 166 Ma (Bridgwater, 1970; Andrews and Emeleus, 1971); however, a new high-precision U–Pb perovskite age of 151.2 ± 1.5 Ma is reported in Frei et al. (2008) for a "kimberlite" dyke from Midternaes in the Pyramidefjeld area.

The Jurassic carbonatite-aillikite magmatism of southern West Greenland is largely confined to the interior parts of the now split NAC (Fig. 1b). There is only minor spatial overlap with Neoproterozoic and Mesoproterozoic carbonatite-aillikite magmatism that occurred at, or close to, the craton margins to the north and south, respectively. All three magmatic episodes are extension-related and produced compositionally very similar carbonatite-aillikite magmas (Larsen and Rex, 1992; Tappe et al., 2007). This suggests that the different segments of the NAC lithospheric mantle experienced a similar CO_2-rich metasomatic impregnation, and radiogenic isotope constraints imply that metasomatism occurred shortly prior to magmatism given the long-term isotopic depletion of these highly trace element enriched carbonatite-aillikite magmas (Nelson, 1989; Pearce and Leng, 1996; Gaffney et al., 2007; Tappe et al., 2007; Tappe et al., 2008a). Furthermore, the apparent lithospheric control on carbonatite-aillikite magmatism, along with the juvenile radiogenic isotope compositions of the produced magmas, suggests melt generation at the lithosphere–asthenosphere boundary during incipient cratonic rifting processes. For example, the Jurassic carbonatite-aillikite magmatism of southern West Greenland (ca. 200–150 Ma) predates the oldest known

terrigenous shelf sediments (Early Cretaceous) offshore West Greenland by only a few million years (Chalmers and Pulvertaft, 2001). It may thus represent the earliest manifestation of the Mesozoic cratonic lithosphere reactivation that occurred along the present-day Labrador Sea margin (Hansen, 1980; Larsen, 2006; Tappe et al., 2007). Based on the temporal evolution and spatial distribution of the carbonate-rich magmatism across southern West Greenland it can be inferred that a thick cratonic root had survived previous Mesoproterozoic and Neoproterozoic extensional stresses. However, it had been significantly thinned during more intensive renewed Mesozoic rifting processes that eventually led to the opening of the Labrador Sea at ca. 60 Ma (Tappe et al., 2007, and references therein). This rather static tectonomagmatic scenario is in contrast to the NW–SE Triassic to Cretaceous age progression that is recognized for kimberlite magmatism across eastern North America (Heaman and Kjarsgaard, 2000). This NW-trending kimberlite corridor is consistent with the relative plate motion of North America during the Mesozoic and interpreted to represent the continental expression of magmatism linked to the Great Meteor mantle plume hotspot track. We therefore conclude that these two contrasting tectonomagmatic scenarios provide evidence for contrasting modes of volatile-rich magma generation; carbonatite-aillikite magma production from metasomatized rifted cratonic mantle (Tappe et al., 2007; Tappe et al., 2008a) as opposed to kimberlite magma production from deeper refertilized subcratonic mantle (Ringwood et al., 1992; Nowell et al., 2004).

4.3. Remarks on carbonatite–kimberlite relationships

Carbonatite–kimberlite relationships have a long history of debate (cf., Mitchell, 1979; Gaspar and Wyllie, 1984), but undoubtedly, some kimberlites differentiate to carbonate-rich rocks, e.g., the Benfontein sill in South Africa, for which Mitchell (1979) suggested the name calcite kimberlite. However, it is imperative to note that none of the global bona fide carbonatite complexes is temporally associated with archetypal kimberlite (Woolley and Kjarsgaard, 2008) and that the so-called central-complex kimberlites of Dawson (1971) are identified as members of the UML group in modern mineralogical–genetic classification schemes (Woolley et al., 1996; Tappe et al., 2005). The West Greenland carbonatite-aillikite occurrences such as Sarfartoq and the newly discovered Tikiusaaq intrusion are prime examples of this carbonatite–UML association.

Nielsen et al. (this issue) and Nielsen and Sand (2008) recently suggested that aillikite magmatism in West Greenland was confined to the strongly metasomatized craton margins, and that there is an increasing "kimberlitic" component in the carbonate-rich magmatism towards the NAC interior. They identified the Majuagaa dyke in the Maniitsoq area, well inside the Archean NAC, as calcite kimberlite based on its groundmass mineralogy and argued that it represents peridotite-contaminated dolomite carbonatite liquid. Although we essentially concur with this interpretation, we urge caution in naming this dyke rock a calcite kimberlite, because it did not differentiate from archetypal kimberlite and does not contain primary serpentine (cf., Mitchell, 2005). We believe that it should be more appropriately referred to as "mantle debris-rich carbonatite" or "carbonatite sensu lato" in order to mitigate against false inferences regarding relationships between rock types formed from magmas of different origins (see also Chakhmouradian et al., this issue). Although the alleged aillikite-kimberlite progression discussed by Nielsen et al. (this issue) refers primarily to the Late Neoproterozoic carbonate-rich magmatism across West Greenland, the data reported here from the Jurassic Tikiusaaq intrusion demonstrate that carbonatite-aillikite magmatism occurred well inside the NAC interior (Fig. 1b). This implies more complex spatial distribution patterns of carbonate–potassic silicate magmatism in structurally complex areas of repeatedly rifted (and metasomatized) cratonic lithosphere; a tectonic environment that is apparently not favourable to the production of bona fide kimberlite magma.

5. Conclusion and outlook

The field observations and geochronology data reported in this study demonstrate that at Tikiusaaq in southern West Greenland carbonatite sheets and dykes, as well as carbonate-rich ultramafic silicate dykes of identical Middle Jurassic age co-occur. This deep volatile-rich magmatism forms part of a larger Jurassic alkaline province in the central part of the now split NAC and appears to be the earliest manifestation of rifting processes related to the opening of the Mesozoic–Cenozoic Labrador Sea Basin. Based on mineral assemblages and compositions, the ultramafic dykes are identified as aillikites and are clearly distinct from macroscopically similar archetypal kimberlites. They strongly resemble the type rocks from Aillik Bay in Labrador and the nearby aillikite dykes from the Sarfartoq carbonatite complex in West Greenland. The carbonate-rich nature of the Tikiusaaq aillikites and their similar age with the associated carbonatites suggest a genetic relationship between these rock types.

Aillikites have the mineralogical characteristics of primitive magmas that carried garnet peridotite xenoliths to the surface; whereas the carbonatite sheets show evidence for differentiation such as evolved olivine microphenocrysts and Fe-rich dolomite compositions. This leads us to reject the commonly invoked melt continuum hypothesis that links dolomite carbonatites, aillikites, and kimberlites by progressively increasing degrees of partial melting of carbonated peridotite at pressures within the diamond stability field. It seems more likely, instead, that proto-aillikite melt was parental to the dolomite carbonatite magma. Testing of the model proposed herein and constraining the mechanism(s) by which proto-aillikite melt can differentiate into carbonatite magma (Tappe et al., 2008b) is the subject of a forthcoming paper that utilizes elemental and isotopic data, as well as geochemical modelling techniques.

Acknowledgments

This work is published with permission of the Geological Survey of Denmark and Greenland. Fieldwork was financially supported by the Bureau of Minerals and Petroleum, Government of Greenland. S.T. acknowledges funding by the Alexander von Humboldt Foundation and L.M.H. acknowledges financial support through an NSERC Discovery grant. Karsten Secher, Karina Sand, and Julie Hollis are thanked for their valuable contributions during fieldwork in the Tikiusaaq area. Sergei Matveev is thanked for maintaining a smoothly operating microprobe facility at the University of Alberta. We appreciate discussions with Troels Nielsen, Rolf Romer, Dejan Prelevic, Zoran Jovanovic, Ilya Veksler, Steve Foley, Vadim Kamenetsky, and Johannes Glodny that ensued during the course of this study. S.T. would like to thank Judy Schultz and Gayle Hatchard for their advice during the geochronology work in Edmonton; and Don Resultay for the many thin section preparation 'rush jobs' he passionately accomplished for this project. We truly appreciate the insightful reviews provided by Hugh O'Brien and Bruce Kjarsgaard.

Appendix A. Supplementary data

Supplementary data associated with this article can be found, in the online version, at doi:10.1016/j.lithos.2009.03.002.

References

Alibert, C., Albarede, F., 1988. Relationships between mineralogical, chemical, and isotopic properties of some North American kimberlites. Journal of Geophysical Research 93 (7), 7643–7671.

Amelin, Y., Zaitsev, A.N., 2002. Precise geochronology of phoscorites and carbonatites: the critical role of U-series disequilibrium in age interpretations. Geochimica et Cosmochimica Acta 66 (13), 2399–2419.

Andrews, J.R., Emeleus, C.H., 1971. Preliminary account of kimberlite intrusions from the Frederikshåb district, South-West Greenland. Report — Geological Survey of Greenland 31, 1–26.
Armstrong, J.P., Wilson, M., Barnett, R.L., Nowicki, T., Kjarsgaard, B.A., 2004. Mineralogy of primary carbonate-bearing hypabyssal kimberlite, Lac de Gras, Slave province, Northwest Territories, Canada. Lithos 76 (1–4), 415–433.
Bell, K., 1998. Radiogenic isotope constraints on relationships between carbonatites and associated silicate rocks: a brief review. Journal of Petrology 39 (11–12), 1987–1996.
Bernstein, S., Kelemen, P.B., Brooks, C.K., 1998. Depleted spinel harzburgite xenoliths in Tertiary dykes from East Greenland: restites from high degree melting. Earth and Planetary Science Letters 154 (1–4), 221–235.
Bernstein, S., Hanghøj, K., Kelemen, P.B., Brooks, C.K., 2006. Ultra-depleted, shallow cratonic mantle beneath West Greenland: dunitic xenoliths from Ubekendt Ejland. Contributions to Mineralogy and Petrology 152 (3), 335–347.
Bizzarro, M., Stevenson, R., 2003. Major element composition of the lithospheric mantle under the North Atlantic craton: evidence from peridotite xenoliths of the Sarfartoq area, southwestern Greenland. Contributions to Mineralogy and Petrology 146 (2), 223–240.
Bizzarro, M., Simonetti, A., Stevenson, R.K., David, J., 2002. Hf isotope evidence for a hidden mantle reservoir. Geology 30 (9), 771–774.
Bridgwater, D., 1970. Routine K/Ar age determinations on rocks from Greenland carried out for GGU in 1970. Rapport Groenlands Geologiske Undersoegelse 35, 52–60.
Brøgger, W.C., 1921. Die Eruptivgesteine des Kristianiagebietes: IV. Das Fengebiet in Telemark. Norwegen. Skrifter udgit av Videnskabsselskabet i Kristiania I. Math.-Nat. Klasse No.9, Kristiania (Oslo). 408 pp.
Chakhmouradian, A.R., et al., 2009, this issue. "Kimberlite" from Wekusko Lake, Manitoba: Actually a diamond-indicator-bearing dolomite carbonatite. Proceedings of the 9th International Kimberlite Conference. Lithos 112S, 347–357.
Chalmers, J.A., Pulvertaft, T.C.R., 2001. Development of the continental margins of the Labrador Sea: a review. In: Wilson, R.C.L., Whitmarsh, R.B., Taylor, B., Froitzheim, N. (Eds.), Non-Volcanic Rifting of Continental Margins: A Comparison of Evidence from Land and Sea. Geological Society of London, London, United Kingdom, pp. 77–105.
Church, A.A., Jones, A.P., 1995. Silicate-carbonate immiscibility at Oldoinyo Lengai. Journal of Petrology 36 (4), 869–889.
Dalton, J.A., Presnall, D.C., 1998. The continuum of primary carbonatitic–kimberlitic melt compositions in equilibrium with lherzolite: data from the system CaO–MgO–Al2O3–SiO2–CO2 at 6 GPa. Journal of Petrology 39, 1953–1964.
Dawson, J.B., 1971. Advances in kimberlite geology. Earth-Science Reviews 7 (4), 187–214.
Emeleus, C.H., Andrews, J.R., 1975. Mineralogy and petrology of kimberlite dyke and sheet intrusions and included peridotite xenoliths from South-west Greenland. Physics and Chemistry of the Earth 9, 179–197.
Fedortchouk, Y., Canil, D., 2004. Intensive variables in kimberlite magmas, Lac de Gras, Canada and implications for diamond survival. Journal of Petrology 45 (9), 1725–1745.
Foley, S.F., et al., 2009, this issue. The composition of near-solidus melts of peridotite in the presence of CO_2 and H_2O between 40 and 60 kbar. Proceedings of the 9th International Kimberlite Conference. Lithos 112S, 274–283.
Frei, D., Gerdes, A., 2009. Precise and Accurate In Situ U–Pb Dating of Zircon with High Sample Throughput by Automated LA-SF-ICP-MS. Chemical Geology 261 (3–4), 261–270.
Frei, D., Hutchison, M.T., Gerdes, A., Heaman, L.M., 2008. Common-lead corrected U–Pb age dating of perovskite by laser ablation — magnetic sectorfield ICP-MS, extended abstract. 9th International Kimberlite Conference, 9IKC-A-00216, Frankfurt.
Friend, C.R.L., Nutman, A.P., Baadsgaard, H., Kinny, P.D., McGregor, V.R., 1996. Timing of Late Archaean terrane assembly, crustal thickening and granite emplacement in the Nuuk region, southern West Greenland. Earth and Planetary Science Letters 142 (3–4), 353–365.
Gaffney, A.M., Blichert-Toft, J., Nelson, B.K., Bizzarro, M., Rosing, M., Albarede, F., 2007. Constraints on source-forming processes of West Greenland kimberlites inferred from Hf–Nd isotope systematics. Geochimica et Cosmochimica Acta 71 (11), 2820–2836.
Garrit, D., Griffin, W.L., O'Reilly, S.Y., 1996. Processes in Archean and Proterozoic mantle in West Greenland. Journal of Conference Abstracts 1 (1), 194 V.M. Goldschmidt Conference.
Gaspar, J.C., Wyllie, P.J., 1984. The alleged kimberlite–carbonatite relationship: evidence from ilmenite and spinel from Premier and Wesselton mines and the Benfontein Sill, South Africa. Contributions to Mineralogy and Petrology 85 (2), 133–140.
Gittins, J., Harmer, R.E., 1997. What is ferrocarbonatite? A revised classification. Journal of African Earth Sciences 25 (1), 159–168.
Gittins, J., Harmer, R.E., 2003. Myth and reality in the carbonatite–silicate rock "association". Periodico de Mineralogia 72, 19–26.
Hansen, K., 1980. Lamprophyres and carbonatitic lamprophyres related to rifting in the Labrador Sea. Lithos 13, 145–152.
Heaman, L.M., Kjarsgaard, B.A., 2000. Timing of eastern North American kimberlite magmatism: continental extension of the Great Meteor hotspot track? Earth and Planetary Science Letters 178 (3–4), 253–268.
Hutchison, M.T., Heaman, L.M., 2008. Chemical and physical characteristics of diamond crystals from Garnet Lake, Sarfartoq, West Greenland: an association with carbonatitic magmatism. The Canadian Mineralogist 46, 1063–1078.
Kjarsgaard, B.A., et al., 2009, this issue. Geochemistry of hypabyssal kimberlites from Lac de Gras, Canada: Comparisons to a global database and applications to the parent magma problem. Proceedings of the 9th International Kimberlite Conference. Lithos 112S, 236–248.
Knudsen, C., Buchardt, B., 1991. Carbon and oxygen isotope composition of carbonates from the Qaqarssuk carbonatite complex, southern West Greenland. Chemical Geology 86 (4), 263–274.
Kretz, R., 1983. Symbols for rock-forming minerals. American Mineralogist 68, 277–279.
Larsen, L.M., 2006. Mesozoic to Palaeogene dyke swarms in West Greenland and their significance for the formation of the Labrador Sea and the Davis Strait. Report — Geological Survey of Denmark and Greenland 34, 1–69 2006.
Larsen, L.M., Rex, D.C., 1992. A review of the 2500 Ma span of alkaline-ultramafic, potassic and carbonatitic magmatism in West Greenland. Lithos 28, 367–402.
Le Maitre, R.W., 2002. Igneous Rocks: A Classification and Glossary of Terms: Recommendations of the International Union of Geological Sciences Subcommission on the Systematics of Igneous Rocks. Cambridge University Press, Cambridge. 236 pp.
Ludwig, K.R., 2000. Isoplot/Ex version 2.2. – a geochronological toolkit for Microsoft Excel. Berkeley Geochronology Center Special Publication No. 1a: Berkeley, California.
Malpas, J., Foley, S.F., King, A.F., 1986. Alkaline mafic and ultramafic lamprophyres from the Aillik Bay area, Labrador. Canadian Journal of Earth Sciences 23, 1902–1918.
Minster, J.F., Birck, J.L., Allegre, C.J., 1982. Absolute age of formation of chondrites studied by the Rb-87–Sr-87 method. Nature 300 (5891), 414–419.
Mitchell, R.H., 1979. The alleged kimberlite–carbonatite relationship: additional contrary mineralogical evidence. American Journal of Science 279 (5), 570–589.
Mitchell, R.H., 1986. Kimberlites: Mineralogy, Geochemistry and Petrology. Plenum Press, New York. 442 pp.
Mitchell, R.H., 1995. Kimberlites, Orangeites, and Related Rocks. Plenum Press, New York. 410 pp.
Mitchell, R.H., 2005. Carbonatites and carbonatites and carbonatites. The Canadian Mineralogist 43 (6), 2049–2068.
Mitchell, R.H., Bergman, S.C., 1991. Petrology of Lamproites. Plenum Press, New York. 447 pp.
Mitchell, R.H., Belton, F., 2004. Niocalite-cuspidine solid solution and manganoan monticellite from natrocarbonatite, Oldoinyo Lengai, Tanzania. Mineralogical Magazine 68 (5), 787–799.
Mitchell, R.H., Scott-Smith, B.H., Larsen, L.M., 1999. Mineralogy of ultramafic dikes from the Sarfartoq, Sisimiut and Maniitsoq areas, West Greenland. In: Gurney, J.J., Gurney, J.L., Pascoe, M.D., Richardson, S.H. (Eds.), Proceedings of the VIIth International Kimberlite Conference. Red Roof Design, Cape Town, pp. 574–583.
Nelson, D.R., 1989. Isotopic characteristics and petrogenesis of the lamproites and kimberlites of central West Greenland. Lithos 22 (4), 265–274.
Nicholls, J., Carmichael, I.S.E., Stormer Jr., J.C., 1971. Silica activity and Ptotal in igneous rocks. Contributions to Mineralogy and Petrology 33 (1), 1–20.
Nielsen, T.F.D., Sand, K.K., 2008. The Majuagaa kimberlite dike, Maniitsoq region, West Greenland: constraints on an Mg-rich silicocarbonatitic melt composition from groundmass mineralogy and bulk compositions. The Canadian Mineralogist 46, 1043–1061.
Nielsen, T.F.D., et al., 2009, this issue. Distribution of kimberlite and aillikite in the Diamond Province of southern West Greenland: A regional perspective based on groundmass mineral chemistry and bulk compositions. Proceedings of the 9th International Kimberlite Conference. Lithos 112S, 358–371.
Nowell, G.M., Pearson, D.G., Bell, D.R., Carlson, R.W., Smith, C.B., Kempton, P.D., Noble, S.R., 2004. Hf isotope systematics of kimberlites and their megacrysts: new constraints on their source regions. Journal of Petrology 45 (8), 1583–1612.
O'Brien, H.E., Tyni, M., 1999. Mineralogy and geochemistry of kimberlites and related rocks from Finland. In: Gurney, J.J., Gurney, J.L., Pascoe, M.D., Richardson, S.H. (Eds.), Proceedings of the VIIth International Kimberlite Conference. Red Roof Design, Cape Town, pp. 625–636.
Patterson, M., et al., 2009, this issue. Kimberlites: Magmas or mixtures? Proceedings of the 9th International Kimberlite Conference. Lithos 112S, 191–200.
Pearce, N.J.G., Leng, M.J., 1996. The origin of carbonatites and related rocks from the Igaliko dyke swarm, Gardar Province, South Greenland: field, geochemical and C–O–Sr–Nd isotope evidence. Lithos 39 (1–2), 21–40.
Peterson, T.D., 1990. Petrology and genesis of natrocarbonatite. Contributions to Mineralogy and Petrology 105 (2), 143–155.
Platt, R.G., Mitchell, R.H., 1979. The Marathon dikes I: Zirconium-rich titanian garnets and manganoan magnesian ulvöspinel-magnetite spinels. American Mineralogist 64, 546–550.
Prelevic, D., Foley, S.F., Romer, R.L., Cvetkovic, V., Downes, H., 2005. Tertiary ultrapotassic volcanism in Serbia: constraints on petrogenesis and mantle source characteristics. Journal of Petrology 46 (7), 1443–1487.
Ringwood, A.E., Kesson, S.E., Hibberson, W.O., Ware, N., 1992. Origin of kimberlites and related magmas. Earth and Planetary Science Letters 113 (4), 521–538.
Rock, N.M.S., 1986. The nature and origin of ultramafic lamprophyres: alnöites and allied rocks. Journal of Petrology 27, 155–196.
Secher, K., Larsen, L.M., 1980. Geology and mineralogy of the Sarfartoq carbonatite complex, southern West Greenland. Lithos 13 (2), 199–212.
Secher, K., et al., 2009, this issue. Timing of kimberlite, carbonatite, and ultramafic lamprophyre emplacement in the alkaline province located 64°–67° N in southern West Greenland. Proceedings of the 9th International Kimberlite Conference. Lithos 112S, 400–406.
Simonetti, A., Heaman, L.M., Hartlaub, R.P., Creaser, R.A., MacHattie, T.G., Böhm, C.O., 2005. U–Pb zircon dating by laser ablation-MC-ICP-MS using a new multiple ion counting Faraday collector array. Journal of Analytical Atomic Spectrometry 20 (8), 677–686.
Simonetti, A., Heaman, L.M., Chacko, T., Banerjee, N.R., 2006. In situ petrographic thin section U–Pb dating of zircon, monazite, and titanite using laser ablation-MC-ICP-MS. International Journal of Mass Spectrometry 253, 87–97.
Stacey, J.S., Kramers, J.D., 1975. Approximation of terrestrial lead isotope evolution by a two-stage model. Earth and Planetary Science Letters 26 (2), 207–221.
Steenfelt, A., Hollis, J.A., Secher, K., 2006. The Tikiusaaq carbonatite: a new Mesozoic intrusive complex in southern West Greenland. Geological Survey of Denmark and Greenland Bulletin 7, 9–12.

Steenfelt, A., Schjøth, F., Sand, K.K., Secher, K., Tappe, S., Moberg, E., Tukiainen, T., 2007. Initial assessment of the geology and economic potential of the Tikiusaaq carbonatite complex and ultramafic lamprophyre dykes. Report — Geological Survey of Denmark and Greenland 64, 1–53 2007.

Tappe, S., Foley, S.F., Jenner, G.A., Kjarsgaard, B.A., 2005. Integrating ultramafic lamprophyres into the IUGS classification of igneous rocks: rational and implications. Journal of Petrology 46 (9), 1893–1900.

Tappe, S., Foley, S.F., Jenner, G.A., Heaman, L.M., Kjarsgaard, B.A., Romer, R.L., Stracke, A., Joyce, N., Hoefs, J., 2006. Genesis of ultramafic lamprophyres and carbonatites at Aillik Bay, Labrador: a consequence of incipient lithospheric thinning beneath the North Atlantic craton. Journal of Petrology 47 (7), 1261–1315.

Tappe, S., Foley, S.F., Stracke, A., Romer, R.L., Kjarsgaard, B.A., Heaman, L.M., Joyce, N., 2007. Craton reactivation on the Labrador Sea margins: 40Ar/39Ar age and Sr–Nd–Hf–Pb isotope constraints from alkaline and carbonatite intrusives. Earth and Planetary Science Letters 256, 433–454.

Tappe, S., Foley, S.F., Kjarsgaard, B.A., Romer, R.L., Heaman, L.M., Stracke, A., Jenner, G.A., 2008a. Between carbonatite and lamproite — diamondiferous Torngat ultramafic lamprophyres formed by carbonate-fluxed melting of cratonic MARID-type metasomes. Geochimica et Cosmochimica Acta 72 (13), 3258–3286.

Tappe, S., Steenfelt, A., Heaman, L.M., Romer, R.L., Simonetti, A., Muehlenbachs, K., 2008b. The alleged carbonatitic–kimberlitic melt continuum: contrary evidence from West Greenland. Geochimica et Cosmochimica Acta 72 (12), A934-A934 Goldschmidt conference abstract, Vancouver, Canada.

Upton, B.G.J., Emeleus, C.H., Heaman, L.M., Goodenough, K.M., Finch, A.A., 2003. Magmatism of the Mid-Proterozoic Gardar Province, South Greenland: chronology, petrogenesis and geological setting. Lithos 68 (1–2), 43–65.

Woolley, A.R., Kempe, D.R.C., 1989. Carbonatites: nomenclature, average chemical compositions, and element distribution. In: Bell, K. (Ed.), Carbonatites: Genesis and Evolution. Unwin Hyman, London, United Kingdom, pp. 1–14.

Woolley, A.R., Kjarsgaard, B.A., 2008. Paragenetic types of carbonatite as indicated by the diversity and relative abundances of associated silicate rocks: evidence from a global database. The Canadian Mineralogist 46, 741–752.

Woolley, A.R., Bergman, S.C., Edgar, A.D., Le Bas, M.J., Mitchell, R.H., Rock, N.M.S., Scott-Smith, B.H., 1996. Classification of lamprophyres, lamproites, kimberlites, and the kalsilitic, melilitic and leucitic rocks. The Canadian Mineralogist 34, 175–186.

Zurevinski, S.E., Heaman, L.M., Creaser, R.A., Strand, P., 2008. The Churchill kimberlite field, Nunavut, Canada: petrography, mineral chemistry, and geochronology. Canadian Journal of Earth Sciences 45 (9), 1039–1059.